SMALL MOLECULE SENSING BY LOCAL PH MODULATION

A Dissertation

by

DA HUANG

Submitted to the Office of Graduate and Professional Studies of
Texas A&M University
in partial fulfillment of the requirements for the degree of

DOCTOR OF PHILOSOPHY

Chair of Committee,	Paul S. Cremer
Committee Members,	Gyula Vigh
	Karen L. Wooley
	Zhilei Chen
Head of Department,	David H. Russell

December 2013

Major Subject: Chemistry

ABSTRACT

Our laboratory has previously invented and characterized a technique for studying ligand-receptor interactions on supported lipid bilayers (SLBs) without fluorescently labeled analytes. This technique utilizes a pH-sensitive dye labeled phospholipid, *ortho*-rhodamine B conjugated POPE (1-hexadecanoyl-2-(9Z-octa-decenoyl)-sn-glycero-3-phosphoethanolamine), as a membrane imbedded reporter molecule to monitor ligand-receptor interactions on SLBs by measuring the fluorescence intensity change. Also, this technique has been demonstrated to operate as either a "turn-on" or a "turn-off" sensor depending on the analytes to be detected. Based on these preliminary studies, it is necessary to give further development and application for this new technique.

Firstly, as a potential application of this sensing technique, we utilized this sensing platform to detect the interactions between tetracaine, a positively charged small molecule used as a local anesthetic drug, and planar supported lipid bilayers (SLBs). Studies with membranes composed of POPC (1-palmitoyl-2-oleoyl-sn-glycero-3-phosphocholine) yielded an equilibrium dissociation constant value of $K_d = 180 \pm 47$ μm for this small molecule-membrane interaction. And the influences of cholesterol, phosphatidylethanolamine, and three negatively charged lipids on the interaction between tetracaine and the bilayers have been studied.

Secondly, in order to fully develop the power of this local pH modulation technique, it has been extended to a homogeneous platform from an SLB based

heterogeneous platform. Specifically, a pH sensitive dye, 5-(and-6)-carboxyfluorescein, was conjugated to free lysine residues on the surfaces of designated capture proteins. The fluorescein intensity was found to change upon target molecule binding. The assay was used to follow the binding of immunoglobulin G (IgG) to streptavidin, thiamin monophosphate (ThMP) to thiamin binding protein A (TbpA), and Ca^{2+} to calmodulin (CaM).

Finally, as an instrumental development for this sensing platform, an inexpensive fluorescence detector has been built as a cheap substitute for the epi-fluorescence microscope. This device is composed of a compact camera, a schott glass color filter, and a green (532 nm) laser pointer. This device has been tested to be able to obtain fluorescence images with decent signal to noise ratio. And this device has been demonstrated in measuring tetracaine-POPC SLB interaction using local pH modulation method.

DEDICATION

This dissertation is dedicated to the people who have been so helpful to me in the past four years. I would not have endeavored such an undertaking without the great support from my wife Yiquan, who is also a chemistry graduate student at Texas A&M University. Also, I would like to dedicate this to my parents, who have always given me solid support. Finally, I would also like to dedicate this to the friends that I have made in the past four years, both within the Cremer group and within the Texas A&M University.

ACKNOWLEDGEMENTS

I would like to thank my advisor, Dr. Cremer, who guide and encouraged me during the whole process. I would also like to thank my committee members, Dr. Russell, Dr. Wooley, and Dr. Chen, for helping me throughout the course of this research.

Thanks also go to Cremer group members, especially Dr. Tinglu Yang who taught me and helped me a lot for all the instruments in the lab, Dr. Tao Zhao, Dr. Chunming Liu, and Dr. Aaron Robinson who collaborated with me on those projects, and Dr. Yangjun Cai and Dr. Zhi Zhao for giving me lots of suggestions during the past four years. I would like to appreciate the rest of the group members, including Xiao Cong, Matt Poyton, Seung-yi Lee, Yi-Ting Liao, Halil Okur, Kelvin Rembert, Anne Sendecki, and Yi Liu for making the group like a big family and leaving me a lot of great memories. I also want to extend my gratitude to my friends and colleagues for making my time at Texas A&M University a great experience.

Finally, thanks to my mother and father for their encouragement and to my wife for her patience and love.

TABLE OF CONTENTS

Page

ABSTRACT ii

DEDICATION iv

ACKNOWLEDGEMENTS v

TABLE OF CONTENTS vi

LIST OF FIGURES viii

LIST OF TABLES x

CHAPTER I INTRODUCTION 1

- Background 1
- Objective 4
- Supported Lipid Bilayers 6
- Microfluidics and Flow Cells 8

CHAPTER II EXPERIMENTAL PROCEDURES AND METHODS 11

- Materials 11
- Experimental for Sensing Small Molecule and Membrane Interactions 14
- Experimental for Sensing Protein and Small Molecule Interactions 19
- Experimental for Inexpensive Fluorescence Detector Fabrication 22

CHAPTER III SENSING SMALL MOLECULES AND LIPID MEMBRANES INTERACTIONS BY LOCAL PH MODULATION 28

- Introduction 28
- Tetracaine-Membrane Interaction Sensing Results and Discussion 34
- Conclusions 54

Page

CHAPTER IV MONITORING PROTEIN-SMALL MOLECULE INTERACTIONS BY LOCAL PH MODULATION 55

Introduction 55
Protein-Small Molecule Interaction Sensing Results and Discussion 59
Conclusions 68

CHAPTER V DESIGN AND ASSEMBLY OF INEXPENSIVE FLUORESCENCE DETECTOR 71

Introduction 71
Inexpensive Fluorescence Detector Fabrication Results and Discussion 74
Conclusions 83

CHAPTER VI CONCLUSIONS 85

REFERENCES 87

LIST OF FIGURES

Page

Figure 1.1 Schematic Diagram of Cell Membrane 2

Figure 1.2 Schematic Diagram of a Supported Lipid Bilayer 7

Figure 1.3 Schematic Diagram of the Sensing System Set up 10

Figure 2.1 Structures of Lipid Utilized in Drug-Membrane Interaction Study 12

Figure 2.2 Structure of Two Dye Molecules 13

Figure 2.3 Schematic Diagram of a Flow Cell for Drug Assays 17

Figure 2.4 Schematic Diagram of a Microfluidic Device 25

Figure 2.5 Inexpensive Fluorescence Microscope Design 26

Figure 2.6 Flow Cell for Inexpensive Fluorescence Detector 27

Figure 3.1 Principles of Drug-Membrane Interaction Sensing 32

Figure 3.2 pH Titration Curves for Different Supported Lipid Bilayers 33

Figure 3.3 Sensing Tetracaine-POPC Bilayer Interaction 36

Figure 3.4 Reversibility Test for Tetracaine-POPC Bilayer Interaction Assay 37

Figure 3.5 Detection Limit Assay 39

Figure 3.6 Cholesterol Influence on Tetracaine-POPC Bilayer Interaction 42

Figure 3.7 Binding Curves for POPE Bilayers 44

Figure 3.8 POPE Influence on Tetracaine-POPC Bilayer Interaction 45

Figure 3.9 Binding Curves for Negatively Charged Lipids Contained Bilayers 48

Figure 3.10 Influence of Negative Charge on Tetracaine-POPC Bilayer Interaction .. 49

Figure 3.11 ITC Data for Tetracaine-POPC Bilayer Interaction 53

Page

Figure 4.1 Principles of Protein-Small Molecule Interaction Sensing 58

Figure 4.2 pH Titration Curves for Labeled Proteins 60

Figure 4.3 rSPA-IgG Binding Induced Fluorescence Intensity Change 62

Figure 4.4 Binding Curves for Protein-Small Molecule Interaction 67

Figure 5.1 Schematic Diagram of Epi-fluorescence Microscopy 73

Figure 5.2 Intensity Scan for Excitation Illumination 75

Figure 5.3 System Characterization 78

Figure 5.4 Application of Inexpensive Fluorescence Detector 79

LIST OF TABLES

Page

Table 4.1 Dissociation Constants for Protein-Small Molecule Interaction..... 66

CHAPTER I

INTRODUCTION

Background

Cell membrane (Figure 1.1), majorly composed of phospholipids, plays important role in cell function and architecture. It protects the cell from its surroundings and supports the embedded proteins. Moreover, through a variety of ligand-receptor interactions, it participates in all kinds of cellular processes such as cell adhesion and cell signaling, which are important for the proper function of a living cell.[1, 2] As a result, being able to monitor ligand-receptor interactions on the cell membrane promotes the understanding of some biological phenomenon and may help discover a broad range of pharmaceuticals with different functions, such as the study of the polyvalent interaction that enables the attachment of an influenza virus to a target cell[3] and the study of interaction between antimicrobial peptide and phospholipid membranes[4, 5]. As demonstrated by some of our group's work, fluorescence technique gives a highly sensitive method in observing these interactions on membrane, which requires the labeling of the protein or peptide.[6-8] Proteins with relative big size might not be affected on its function or activity, as those labeled dye molecules could be located at the places that are not crucial to the protein function. However, for small proteins and peptides, fluorescent dye molecules could have altered the structure and the function of the protein or peptide, which in turn voids the assay's result.[9] Also, the high cost for some photo-stable and bright dye molecules as well as the time effort in labeling and separation process make this technique less not efficient.[10, 11]

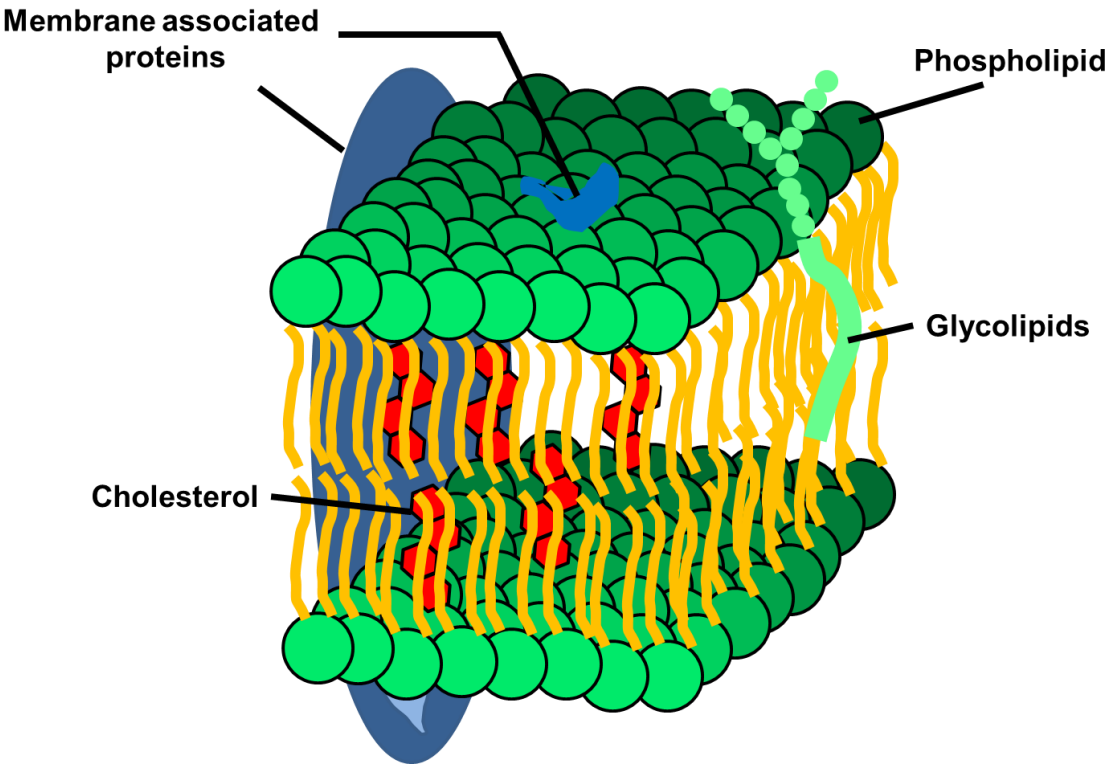

Figure 1.1. Schematic Diagram of Cell Membrane. The graph schematically illustrates a cell membrane with common components, including phospholipid, glycolipid, cholesterol and some membrane associated proteins.

To address these deficiencies of this fluorescence technique based on dye labeling, various methods have been developed and applied on detecting ligand-receptor interaction on model cell membranes. These methods include the use of Surface Plasmon Resonance (SPR),[12-15] Surface Enhanced Raman Scattering (SERS),[16, 17] Quartz Crystal Microbalance with Dissipation monitoring (QCM-D),[18, 19] micro-cantilevers,[20, 21] micro-calorimetry[22], Second Harmonic Generation (SHG),[23] Sum Frequency Generation Vibrational Spectroscopy (SFG-VS)[24], and so on. Although these techniques in deed provide alternative label-free ways in detecting membrane based ligand-receptor interaction, they can be costly, less efficient, less sensitive, and difficult to be applied in membranes based studies.

Recently, a label-free fluorescence based technique has been invented and characterized in our group, which monitors the ligand-receptor interaction on supported lipid bilayer (SLB),[25] a model membrane formed on the surface of borosilicate glass cover slips.[26] Specifically, a pH sensitive dye, *ortho*-conjugated Texas Red DHPE was incorporated into an SLB. *Ortho* isoform of this fluorescent dye loses its fluorescence intensity upon de-protonation under high environment pH. On the other hand, *para* isoform of this molecule gives no response to the environment pH, which serves as a good reference. Also, any ligand molecule that could be linked to a lipid molecule, such as biotin-PE (1,2-dipalmitoyl-sn-glycero-3-phosphoethanolamine-N-(cap biotinyl) (sodium salt)), could be accommodated inside the SLB. Upon the binding of the target molecule, such as anti-biotin IgG, increased fluorescence intensity could be observed. The assay shows the sensitivity with 5 orders of magnitude lower than K_d. Later on,

Robison et al.[27] have demonstrated that a different dye, *ortho*-conjugated Rhodamine B, could also be utilized in this assay, which has lower pK_a that is closer to physiological pH. And this assay could be run in either turn-on mode or turn-off mode, depending on the charge status on the target molecule. By manipulating the ionic strength of the operating buffer, it is also possible to widen the sensing pH range in order to accommodate more target molecules with different pK_a values.

Objective

Considering the advantages that have been demonstrated by previous group members of this pH modulation technique, it is necessary to give further development and find possible real applications on it. Firstly, a great number of small drug molecules currently on the market target membrane localized proteins, such as receptors and ion channels.[28, 29] These molecules can also directly or indirectly interact with the surrounding lipid membrane,[30-33] which may lead to changes in a drug's function and properties.[34] Thus, it is important to understand the intrinsic interactions between drug molecules and lipid membranes. As most drugs are small molecules, whose properties may be altered greatly upon fluorescent labeling, it is imperative to employ label free methods to study small molecule-membrane interactions. Thus, we wish to utilize the fluorescence based pH modulation technique as a simple and novel label free method to observe the interaction between drug molecules and model lipid bilayer and extract thermodynamic data. On the other hand, considering new drug development industry might be most in need of such a technique that could help screen out the most useful new

drug molecule, flow cell with patterned SLBs is utilized. This enables the potential to explore multiple membrane interactions on the same device at the same time.

Secondly, measurements of the affinity between biomolecules, such as protein-protein interactions, protein-small molecule interactions, and protein-ion interactions not only provide insight into basic cellular processes but can also facilitate the development of therapeutics and serve as the basis for many diagnostic techniques.[35] Homogeneous methods, such as ITC, have been commonly utilized. However, in the case of small molecule weakly binding, the heat generated could be very tiny that might not be detected. While for Interfacial methods, such as Surface Plasmon Resonance (SPR),[36, 37] microcantilever sensing,[38] and nanowire sensing,[39] the requirement of immobilizing biomolecules onto surfaces can potentially cause problems even though they permit detection down to the pM level and sometimes below it. For example, the receptor sites on a protein might face the surface, inhibiting the binding process. Also, surface immobilization could alter the conformation and activity of the immobilized protein via partial or complete denaturation.[40] As such, we were wondering whether it is able to extend and develop our interfaced based sensing platform to a solution based homogeneous sensing platform, enabling the sensing of these interactions. In this extended sensing platform, the protein works as the matrix like the SLB, while the binding pocket works as the ligand that was accommodated in the bilayer. The pH sensitive dyes get randomly labeled to the free amines on the protein backbone in sensing the local pH change that might be induced by the binding event.

Finally, the device that we utilized for monitoring the fluorescence intensity of those label-free assays was fluorescence microscope. However, a fluorescence microscope is very expensive that costs tens of thousands of dollars. Also, the size and weight of a fluorescence microscope make it very inconvenient to carry out a fluorescence intensity measurement outside the lab. With a brief research over the web, the commercialized cameras, schott glass filters, and the laser pointers has been so well developed with pretty low price on market. Actually, these things could be good substitute for key components in a fluorescence microscope. Also, the schott glass filters and the COMS chip in a camera have been reported to be successfully integrated onto hand-held devices.[41-43] Thus, we were engaging in designing and building up a family affordable and portable fluorescence detector cost under couple hundred dollars.

Supported Lipid Bilayers

Supported lipid bilayers (SLBs), as shown in Figure 1.2, are one of the model cell membrane systems. They have been widely used as model cell membranes in vitro,[44, 45] as they have the similar lipid composition and could maintain the two-dimensional lipid fluidity.[26] Moreover, their composition could be modulated to accommodate certain ligands, phospholipid, and other species. The SLBs could be formed through a spontaneous fusion method with high repeatability.[46, 47] The size of the SLBs are around 40-50 Å in thickness with a central lipid hydrocarbon chain around 30 Å and a thin water layer (10-20 Å) existing between the lower leaflet and the solid support.[48-50] They could be put in microfluidic devices[51] or patterned[52, 53] in a flow cell, enabling the multiplexed assays.

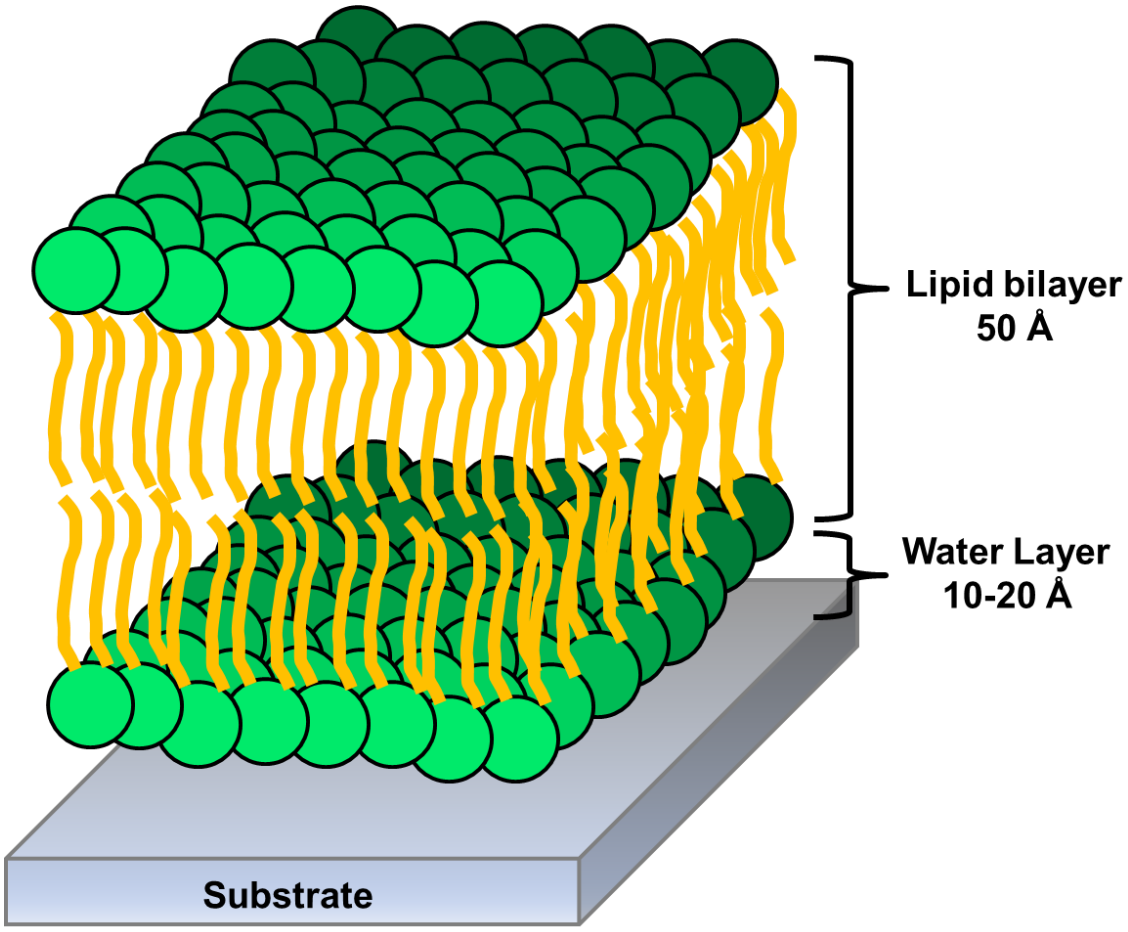

Figure 1.2. Schematic Diagram of a Supported Lipid Bilayer. The substrate in the all the experiment here is borosilicate glass. A thin water layer that is around 1-2 nm thick underneath the bilayer helps keep the two dimensional fluidity of the lipid bilayer.

Microfluidics and Flow Cells

Microfluidic devices have been widely utilized in the field of drug discovery,[54] proteomics,[55] neural cell biology,[56] et al. In our group, we utilize Polydimethylsiloxane (PDMS) to fabricate microfluidic devices in a rapid way.[57] Briefly, a PDMS mold is fabricated via soft lithographic techniques.[58] With its channel size in less than several hundred microns both in length and depth, it requires very small sample volumes to fill up the whole channel. In addition, with the multiple (usually 2-7) integrated channels on a single microfluidic device, it offers the advantage of multiplexing many bilayer studies simultaneously, which could greatly save the time and effort in taking assays under different conditions. Also, set a channel as a standard for the illumination control will help reduce the noise coming from the temporal unstable illumination from the lamp.

Another device designed for the sensing platform is a flow cell made of circular PDMS wells. Patterned lipid bilayer could be made in the well, enabling the multiplexed sensing. Although a flow cell has relatively large dead volume and longer sensing time compared to a microfluidic device, it helps to avoid some potential problems caused by PDMS.[59]

Previously, when the target molecules are labeled by dye molecules in bilayer studies in microfluidics, the unbounded target molecules in bulk solution could give huge fluorescence background. In order to reduce this background, total internal reflection fluorescence microscopy (TIRFM) was utilized. [7, 8, 60] However, TIRFM requires lots of extra set up compared to an epi-fluorescence microscopy. For example, it requires a laser with correct wavelength and a line generator that can give a straight line shaped illumination over the multiple channels on the microfluidic device. Also, a dove prism is needed to adjust

the illumination angle to achieve total internal reflection. Besides, between the dove prism and the microfluidic device, index matching oil needs to be utilized, which makes the device slippery and difficult to be fixed in place. With the development of previously descripted label free pH modulation technique, it is possible to switch back to a common epi-fluorescence microscopy with the device located on the sample stage. The mounted mercury lamp and the filter set could be used for the fluorescence excitation illumination, while the mounted deep cooled CCD camera could be utilized to monitor the fluorescence intensity. A gradient flow is adopted for the flushing and switching of the solutions in the device. The schematic set up is shown in Figure 1.3.

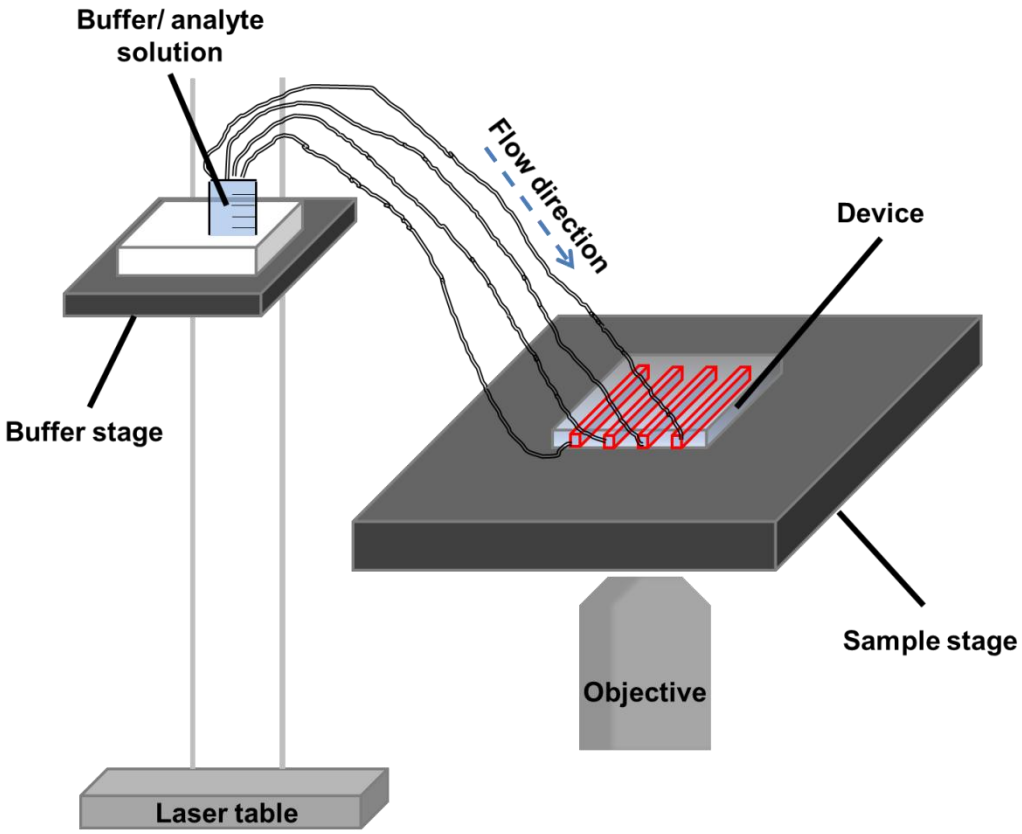

Figure 1.3. Schematic Diagram of the Sensing System Set up. The buffer is flowed into the device mounted on the sample stage though gradient force. The flow speed could be adjusted by the height of the buffer stage. The fluorescence intensity of the device is monitored in real time by an epi-fluorescence microscopy. The drawing is not to scale.

CHAPTER II

EXPERIMENTAL PROCEDURES AND METHODS*

Materials

1-palmitoyl-2-oleoyl-sn-glycero-3-phosphocholine (POPC), 1-palmitoyl-2-oleoyl-sn-glycero-3-phosphoethanolamine (POPE), 1-palmitoyl-2-oleoyl-sn-glycero-3-phospho-(1'-rac-glycerol) (sodium salt) (POPG), 1-palmitoyl-2-oleoyl-sn-glycero-3-phospho-L-serine (sodium salt) (POPS), ganglioside GM1 and cholesterol were purchased from Avanti Polar Lipids (Alabaster, AL). The chemical structure of all the lipids utilized here, including *ortho*-rhodamine B conjugated POPE (oRB-PE) and *ortho*-rhodamine B conjugated biotin (oRB-biotin) are shown in Figure 2.1. The preparation of oRB-PE and oRB-biotin are described in the next section.

Lissamine rhodamine B sulfonyl chloride (mixed isomers) (Figure 2.2(a)) were purchased from Invitrogen (Eugene, OR). (5-and-6)-carboxyfluorescein, succinimidyl esters (mixed isomers) (5(6)-FAM-SE) (Figure 2.2(b)) were purchased from Invitrogen (Carlsbad, CA). Tetracaine came from Sigma-Aldrich (Saint Louis, Missouri). Fibrinogen came from MP Biomedicals (Solon, OH).

---

* Part of the data reported in this chapter is reprinted with permission from *Biosens. Bioelectron.*, 38, Huang, D.; Robison, A. D.; Liu, Y.; Cremer, P. S., "Monitoring protein–small molecule interactions by local pH modulation", 74-78, Copyright 2012, with permission from Elsevier.

* Part of the data reported in this chapter is reprinted with permission from "Sensing Small Molecule Interactions with Lipid Membranes by Local pH Modulation" by Huang, D.; Zhao, T.; Xu, W.; Yang, T.; Cremer, P. S. *Anal. Chem.* [Online early access]. DOI: 10.1021/ac401955t. Published Online: Oct. 23, 2013. Copyright 2013 American Chemical Society.

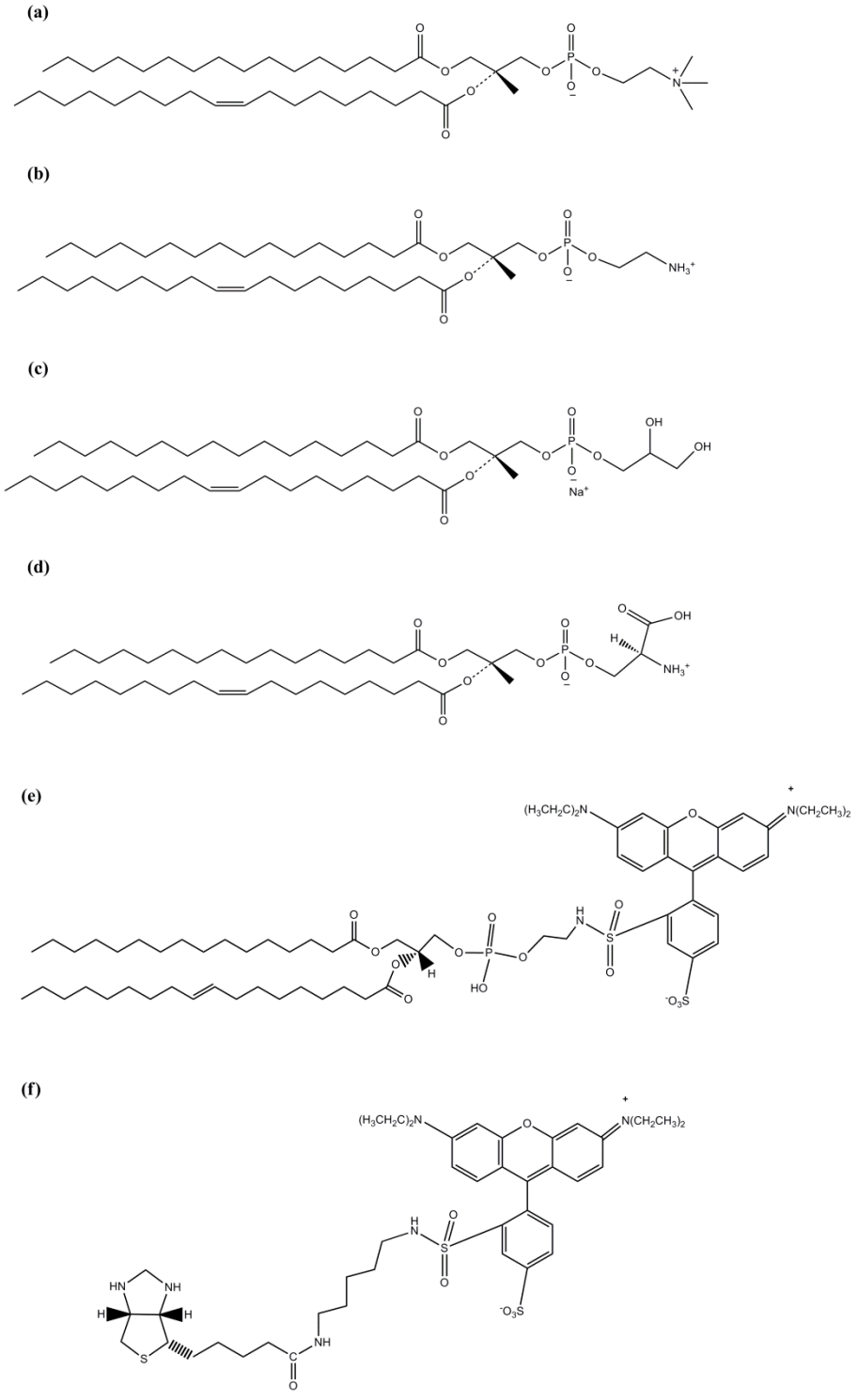

Figure 2.1. Structures of Lipid Utilized in Drug-Membrane Interaction Study. They are (a) POPC, (b) POPE, (c) POPG, (d) POPS, (e) oRB-PE, and (g) oRB-biotin.

(a)

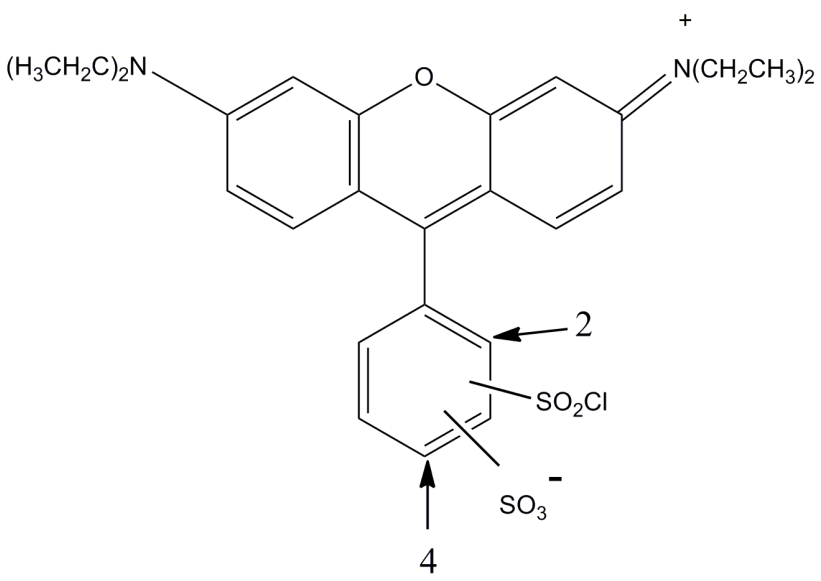

(b)

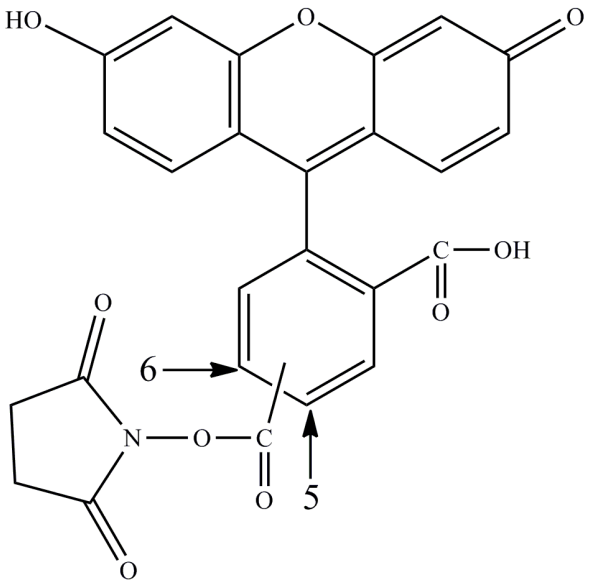

Figure 2.2. Structure of Two Dye Molecules. The figure shows the structure of (a) lissamine rhodamine B sulfonyl chloride (mixed isomers) and (b) (5-and-6)-carboxyfluorescein, succinimidyl esters (mixed isomers).

Native recombinant Staphylococcal aureus Protein A was obtained from Syd Labs (Malden, MA). Human IgG, bovine calmodulin and thiamin monophosphate were purchased from Sigma-Aldrich (St. Louis, MO). Bovine calmodulin and thiamin monophosphate were purchased from Sigma-Aldrich (St. Louis, MO). Thiamin binding protein A was supplied by the Begley laboratory at TAMU. Bio-Spin columns with Bio-Gel P-6 were obtained from Bio-Rad (Hercules, CA). Hydrofluoric acid is from EMD (Philadelphia, PA). Ammonium fluoride was obtained from Alfa Aesar (Ward Hill, MA).

Purified water was produced from a NANOpure Ultrapure Water System (18.2 MΩ·cm, Barnstead, Dubuque, IA). Microscope slides (25 ×75 ×1.0 mm) were obtained from Fisher Scientific (Pittsburgh, PA). Glass coverslips (24 × 40 mm, No. 1.5) were from Corning Inc. (Corning, NY). PDMS was purchased from Krayden, Inc (El Paso, TX). Thin layer chromatography (TLC) plates (silica gel 60 F254) were obtained from EMD (Philadelphia, PA). Polytetrafluoroethylene (PTFE) tubing (inner diameter approximately 0.66 mm) was purchased from Newark/element 14 (Palatine, IL). Schott colored glass filter (25.4 mm Diameter, Cut-on 570 nm, OG.570) was purchased from Newport (Bozeman, MT). 532 nm laser pointer was obtained from Newegg Inc. (Whittier, CA).

Experimental for Sensing Small Molecule and Membrane Interactions

Rhodamine B-POPE and Rhodamine B-Biotin Preparation and Purification. 10 mg rhodamine B sulfonyl chloride dissolved in 1 ml anhydrous chloroform was added drop by drop to 10 mg/ml POPE in chloroform in an ice bath. After this, 2 μL triethylamine was added to the mixed solution. The reaction was stirred for 4 hours at

room temperature. After the reaction, the mixture was spotted onto a TLC plate (EMD, 5715-7, silica gel 60 F254), blown dry with nitrogen gas, and developed with a chloroform-methanol mixture (92:8 by volume) to separate rhodamine-B labeled POPE mixed isomers from the reactants. The rhodamine B-POPE mixed isomers were then separated from each other on another TLC plate developed with a mixture of ammonium hydroxide solution, dichloromethane, and n-propanol (5:60:35 by volume). Each separated band on the TLC plate was scratched off with a razor blade and collected onto a column. A mixture of chloroform and methanol (7:3 by volume) was utilized to elute the dye-conjugated lipids from the surface. The concentration of each isomer of rhodamine B-conjugated POPE was measured by UV-Vis.

The preparation and purification of the oRB-biotin conjugate was done in a manner analogous to the preparation of oRB-POPE. In this case, 5 mg/ml pentylamine-biotin (Fisher Scientific, Pittsburgh, PA) was used instead of POPE.

Small Unilamellar Vesicles (SUVs) Preparation. Lipids were mixed at the desired mole ratio in chloroform in a glass vial. Afterward, the chloroform was removed by continuous purging with nitrogen. Desiccation was then performed under vacuum for more than 2 h to remove any residual organic solvent. The dried lipid films were hydrated with 10 mM phosphate-buffered saline (PBS) containing 150 mM NaCl, followed by sonication in a bath to obtain 0.5 mg/ml lipid suspensions. These suspensions were then subjected to at least 7 freeze-thaw cycles with liquid nitrogen and water (room temperature) and at least 7 extrusion cycles through two stacked 100 nm polycarbonate membranes (Whatman) using a Lipex extruder (Northern Lipids Inc.

Vancouver, Canada). The size of the lipid vesicles was about 95 ± 10 nm as determined by dynamic light scattering measurements (Brookhaven Instruments 90Plus Particle Size Analyzer). The newly prepared SUV solutions were stored at 4 ℃ until use.

Cover Slip Treatment Procedure. All glass cover slips employed for bilayer formation were first cleaned in a near boiling mixture of ICN 7X detergent (Costa Mesa, CA) and purified water (1:4 volume ratio), followed by rinsing the cover slips sequentially with purified water and ethanol at least 3 times. The coverslips were then dried under flowing nitrogen and annealed at 530 °C for 5 h in a kiln (Sentry Xpress 2.0, Orton Ceramic Foundation, OH), which render the surface of the glass smooth and hydrophilic.

Flow Cell Fabrication. For a flow cell device, as shown in Figure 2.3, a polydimethylsiloxane (PDMS) cover block served as the ceiling of the device. Two small holes in this block served as inlet and outlet ports for flowing liquid. The PDMS block was placed directly over a second thin PDMS film (0.52-0.64 mm) with an 8 mm diameter hole in the middle that defined the exposed area of a No. 2 glass coverslip placed beneath it. Flowing aqueous solutions came into contact with this exposed area. Two thin stainless steel plates (6.5 cm by 3.0 cm) with a 1.0 cm diameter hole in the center clamped the entire flow cell together.

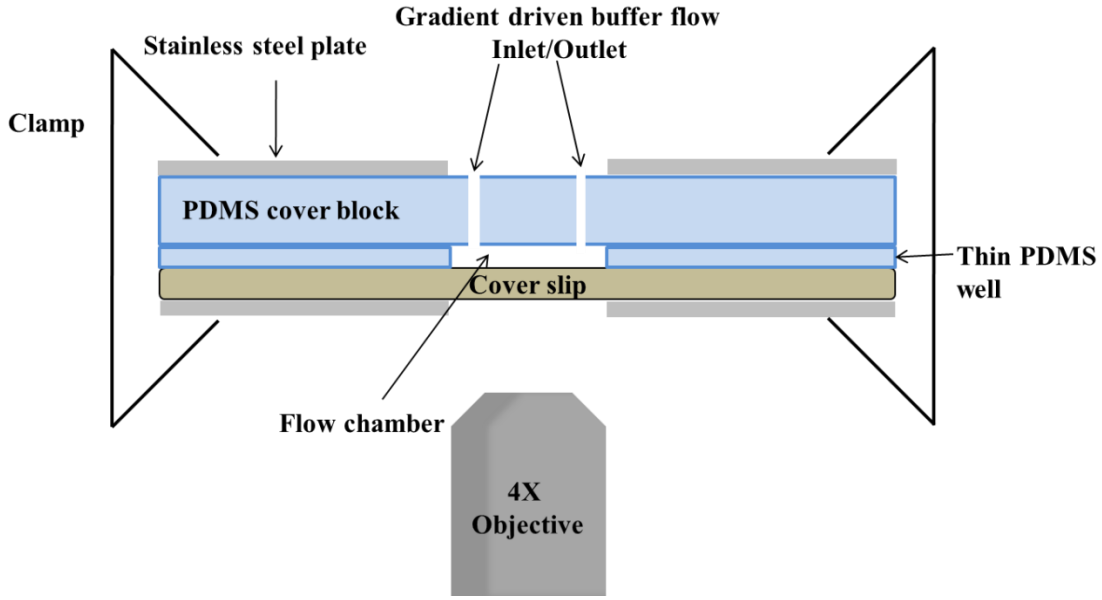

Figure 2.3. Schematic Diagram of a Flow Cell for Drug Assays. The size of the stainless steel plate is 6.5 cm by 3 cm, with the center round window at 1 cm in diameter. The PDMS cover block, PDMS well and coverslip fit right in between those two stainless steel plates. The SLB is coated on the lower glass slide. The drawing is not to scale.

The thin PDMS film used in the flow cell was fabricated by curing PDMS in between two silanized glass plates with a spacer of 4 stacked No. 1 cover slips (100-150 μm thick) and trimmed to the correct size to fit the flow cell. A round section was cut out to form the well. The thicker PDMS cover block was made the same way except that a 4 mm thick spacer was used instead. Two holes were reamed into this block by the tip of a hollow needle.

PDMS Stamp and Patterned SLBs. After placing the thin PDMS film on a cover slip surface, lipid bilayers were patterned in stripes onto the glass inside the circular PDMS hole. Such patterning provided a simple method for comparing signal changes in the SLBs with the background fluorescence intensity during an experiment. To do this, a PDMS stamp was formed by curing initially uncrosslinked PDMS overnight over a patterned glass mold at room temperature,[61] which is similar to the preparation of the PDMS for the microfluidic device. The glass mold had a series of 380 μm × 1 cm parallel lines spaced 200 μm from each other that were fabricated by HF etching. The PDMS stamp was then cut into appropriately sized sections that would just fit inside the PDMS well in the flow cell. Once cured, the molds were soaked overnight in hexane to remove any uncured PDMS. They were then dried at room temperature and rinsed with ethanol and purified water.

To obtain patterned SLBs, the PDMS stamps were put into conformal contact with the glass surface in the flow cell and fixed in place with a piece of tape. Next, a 1 mg/ml fibrinogen solution was injected into the well and incubated for 5 min, forming a fibrinogen monolayer on the uncovered portions of the glass. The fibrinogen solution

was washed away in a 150 mM NaCl solution before peeling off the PDMS stamp. Finally, the desired lipid vesicle solution was introduced into the well. This caused supported lipid bilayers to form by vesicle fusion to the portions of the glass support that were not blocked by the protein monolayer.[46, 62] After this, the PDMS block was introduced to close the chamber in finishing fabrication of the flow cell.

pH Titration Curves. Experiments were performed to obtain titration data for 0.5 mol% *ortho*-rhodamine B-POPE in POPC bilayers as well as this bilayer containing 20 mol% POPE, 20 mol% Cholesterol, and 20 mol% POPS. The pH of the bulk solution above the bilayers was altered via the continuous flow of pH adjusted by 50 mM phosphate buffer. The fluorescence intensity was monitored till a steady state. According to the titration data, pH 7.1 was selected as it falls within the pH response range of dye molecule and is close to physiological pH.

Fluorescence Microscopy. A Nikon Eclipse Ti-U fluorescence microscope (Tokyo, Japan) equipped with a ProEM 1024 CCD camera (Princeton Instruments) and Lumen 200 (Prior Scientific) light source was utilized to take fluorescence images. A 4X air objective (N.A. = 0.45) was used for imaging along with a Texas Red filter set (Chroma Technology, Bellows Falls, VT). MetaMorph software (Version 7.7.0.0, Universal Imaging) was employed to process the images.

Experimental for Sensing Protein and Small Molecule Interactions

Protein Labeling Procedure. TbpA solutions were made with 10 mM phosphate buffered saline (PBS) at pH 7.2 and a protein concentration of 2 mg/ml. The buffer contained 150 mM NaCl and 1 mM NaN_3. To label the proteins, 20 μL of 1 M Na_2CO_3

was added to 100 μL of a 2 mg/ml protein solution. Next, 0.3 mg of 5(6)-FAM-SE were added to the solution and stored at 4 ° C for 2 days. Subsequently, the labeled proteins were separated from remaining free dye molecules via Bio-Spin columns with Bio-Gel P-6.

Calmodulin was reconstituted from a lyophilized powder by 50 mM HEPES buffer containing 150 mM NaCl and 1 mM EGTA to a final concentration of 2 mg/ml. 5 μL of 1 M Na_2CO_3 and 1 μL of 10 mg/ml 5(6)-FAM-SE DMSO solution were sequentially added to a 50 μL calmodulin solution. The solution was then stored at 4° C overnight. Finally, remaining free dye was removed from the labeled protein with a Bio-Spin column before use.

pH Titration Curve Measurements. 100 mM Tris/Citrate buffer was prepared at pH values ranging from 4.0 to 6.5 by adjusting the pH with NaOH/HCl. 100 mM Tris buffer was prepared at pH values ranging from 7.0 to 11.0 by adjusting the pH with NaOH/HCl. These pH values were chosen to locate the pKA value of the fluorescein dye conjugated to each protein. The pH was obtained with a standard glass electrode setup with measurements having an error of ± 0.1 pH units. Titration curves for the dye molecules on the proteins were made by adding 5 μL of a fluorescein-labeled protein solution to 95 μL of buffer. Fluorescence emission spectra were obtained by a QE 65000-FL Scientific Grade Spectrometer (Ocean Optics, Dunedin, FL) by setting the excitation peak to 488 nm.

Binding Measurements. For fluorescein-labeled TbpA binding to ThMP, 1 μL of 1.67 mg/ml dye-labeled TbpA was added to 2 ml of 100 mM Tris/50 mM citrate buffer

at pH 6.5 in a QVFL-Q-10 cuvette. In this case, aliquots of 25 μM ThMP in water were added to the cuvette to generate different concentrations of ThMP with a 15 min room temperature incubation allowed before each measurement. For fluorescein-labeled CaM binding to Ca^{2+}, 6 μL of 1.54 mg/ml 5(6)-FAM labeled CaM was added to 94 μL of 50 mM HEPES buffer containing 150 mM NaCl and 1 mM EGTA at pH 6.8 in a type 703M Cuvette (Precision Cell, Farmingdale, NY). Aliquots of either 10 mM or 100 mM $CaCl_2$ were introduced stepwise to generate different free Ca^{2+} concentrations with a 1 min incubation period at 25 ° C allowed before each measurement. All fluorescence emission spectra were obtained with a QE 65000-FL Scientific Grade Spectrometer by setting the excitation peak to 488 nm.

Error analysis of the emission intensity was performed. The fluorescence intensity of labeled TbpA protein diluted in buffer solution in a cuvette was found to be stable to within 0.4% over 10 min of continuous excitation in the fluorometer. In another control, ThMP was introduced into a solution of TbpA and free dye, which led to almost no signal change. Moreover, 100 nM biotin and 100 nM adenosine monophosphate (AMP) molecules, respectively were introduced to a labeled TbpA solution. This gives no signal, indicating that fluorescence modulation is selective to the specific target molecule. Is this a repeat of the paragraph below?

CaM-Ca^{2+} binding measurements described herein have been accompanied by control experiments that utilized free dye in solution instead of labeled proteins to establish that the signal was indeed due to the putative binding event rather than changes in fluorescence caused by dye-analyte interactions. Almost no signal changes were

observed in the presence of ThMP. For Ca^{2+}, the control assays gave rise to an approximately 1% intensity decrease in fluorescence at the highest Ca^{2+} concentration employed. This change was probably due to a slight decrease in the bulk pH rather than any direct Ca^{2+}-fluorescence interaction. In fact, the change was linear with pH and could easily be distinguished from the Langmuir isotherm response due to CaM-Ca^{2+} interactions.

Experimental for Inexpensive Fluorescence Detector Fabrication

Fabrication of Microfluidic Device. After soak the Glass slides (soda lime, Corning) in a mixed 1:3 (v/v) concentrated hydrogen peroxide and concentrated sulfuric acid solution for at least one hour, the slides were rinsed with deionized distilled water thoroughly and dried with nitrogen. A thin layer of photoresist (Shipley 1823) was spin-coated onto the glass slides with several hundred microns in thickness. With a previously designed mask attached to the photoresist side of the slide, the slides were exposed to UV (> 400 W) for 8-12 seconds after a hard baking procedure (115 ^{o}C, 1.5 min). A developing solution and acetone was then utilized to remove all the exposed photoresist. Later on, the glass slides were blew dry and underwent another hard baking process (115 ^{o}C, 1.5 min).

Buffered oxide etchant (BOE) solution was prepared by mixing a 1:6 ratio (v/v) of 48% hydrofluoric acid (EMD Chemicals Inc., Germany) and aqueous ammonium fluoride (200 g in 300 mL purified water, Alfa Aesar, Ward Hill, MA), which was used to etch the patterns into the glass slides. The glass was immersed into the BOE solution for 2-3 min and 1 M hydrochloride acid solution for 1 min sequentially, which should be

repeated at least 4 times before remove the photoresist. After that, the slides were coated with triflorododecylsilane.

PDMS was prepared by mixing 10:1 (v/v) of Sylgard silicone elastomer-184 and the curing agent, degassed under vacuum before it was poured over the patterned glass slides. Then, the PDMS got annealed in a 65 ^{o}C oven over night. After treating both the annealed PDMS and the cover slip were treated with 25 W oxygen plasma for 60 seconds, the PDMS was brought into contact with the cover slip. A microfluidic device could be obtained as shown in Figure 2.4.

Fabrication of Inexpensive Fluorescence Detector. The 532 nm laser pointer was directly connected to a 3 V DC power supply (Agilen Inc., Englewood, CO) and was kept on to give a constant laser out put approximately at 12 mW. The laser pointer was mounted on the laser table with a tilted angle to the sample stage in order to avoid the direct reflection of the laser light into the camera lens. The schott glass filter (OG. 570) was attached to the lens of the camera by double side tape. Black insulation tape was utilized to seal the gap between the filter and the camera lens, which might cause the leak of light. The camera was just located in front of the sample stage at the same height, which was approximately 6 cm, in order to collect as much light as possible while still enables manual focusing. The buffer or analyte solution stage is mounted relatively higher than the sample stage for the purpose of gradient driven flow. For an intuitive view of the designed device, a schematic figure and a picture for the real device are shown in Figure 2.5.

Fabrication of Flow Cell. Here, the flow cell is modified based on the flow cell previously described. As shown in Figure 2.6, two cover slips served as the ceiling and the bottom of the device respectively. A polydimethylsiloxane (PDMS) cover block served as the spacer of the device that defines the well volume. Two small holes on either side of this block served as inlet and outlet ports for flowing liquid. The PDMS block was placed directly over a second thin PDMS film (0.52-0.64 mm) with an 8 mm diameter hole in the middle that defined the exposed area of a No. 2 glass coverslip placed beneath it. Flowing aqueous solutions came into contact with this exposed area. One thin stainless steel plates (6.5 cm by 3.0 cm) with a 1.0 cm diameter hole in the center was utilized to reinforce the bottom cover slip. And the whole device is clamped together. The thin PDMS film and the thicker PDMS cover block was made the same way except as previously described.

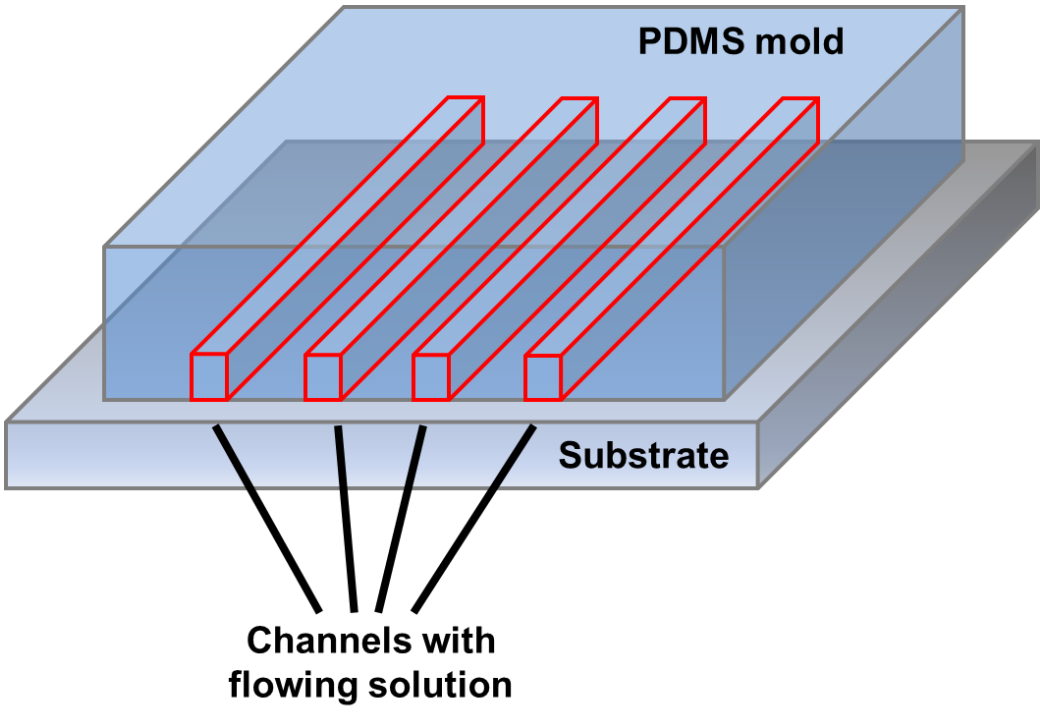

Figure 2.4. Schematic Diagram of a Microfluidic Device. The PDMS mold and cover slip substrate is covalently bound together. The number of channels within the device usually could be made from 2-9 depending on demand.

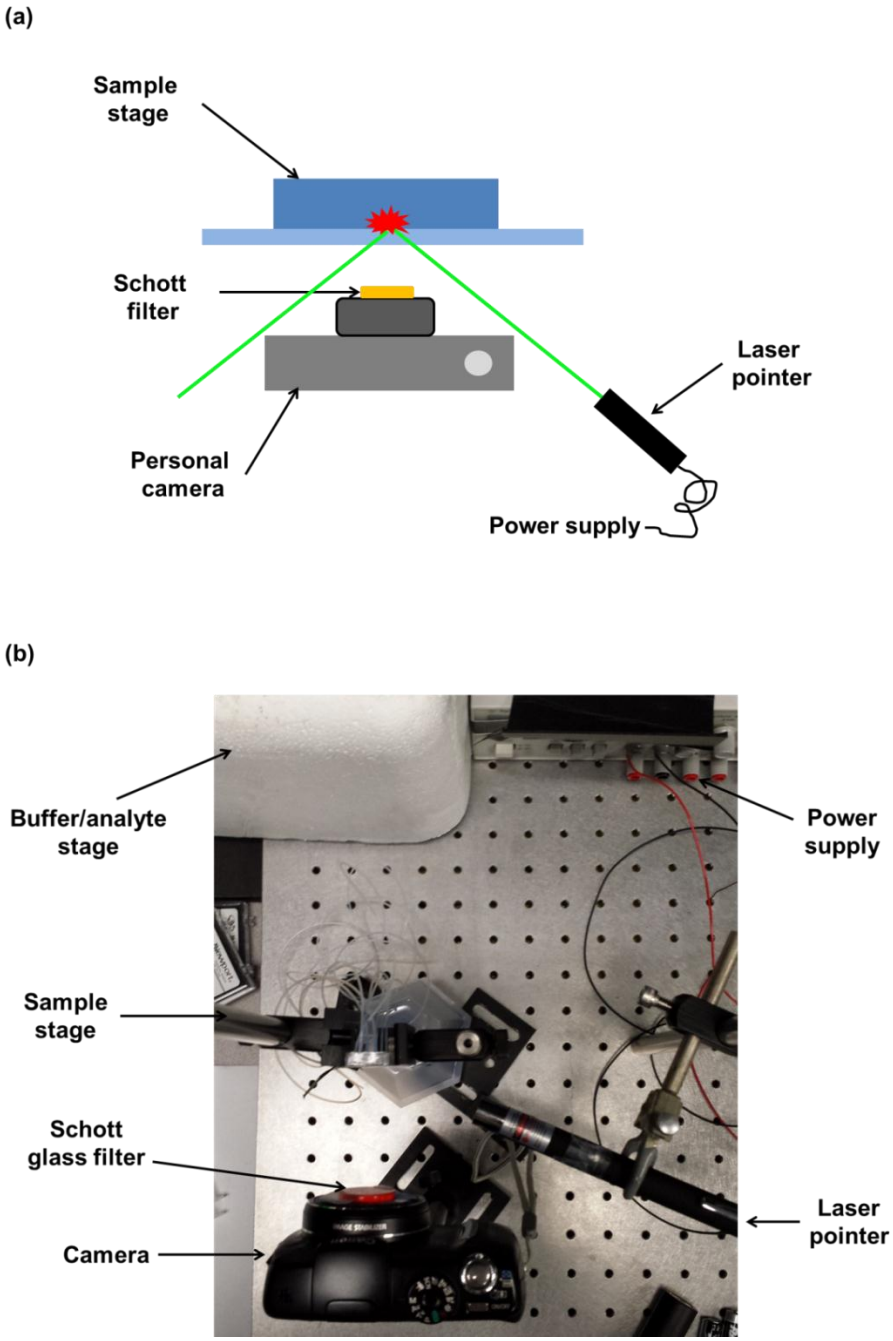

Figure 2.5. Inexpensive Fluorescence Microscope Design. (a) The schematic graph that shows the design of the inexpensive fluorescence detector. (b) The real picture of the assembled inexpensive fluorescence detector. The laser pointer was mounted tilted to the sample stage to avoid the direct reflection of laser light into the camera. On the sample stage, a microfluidic device is mounted here.

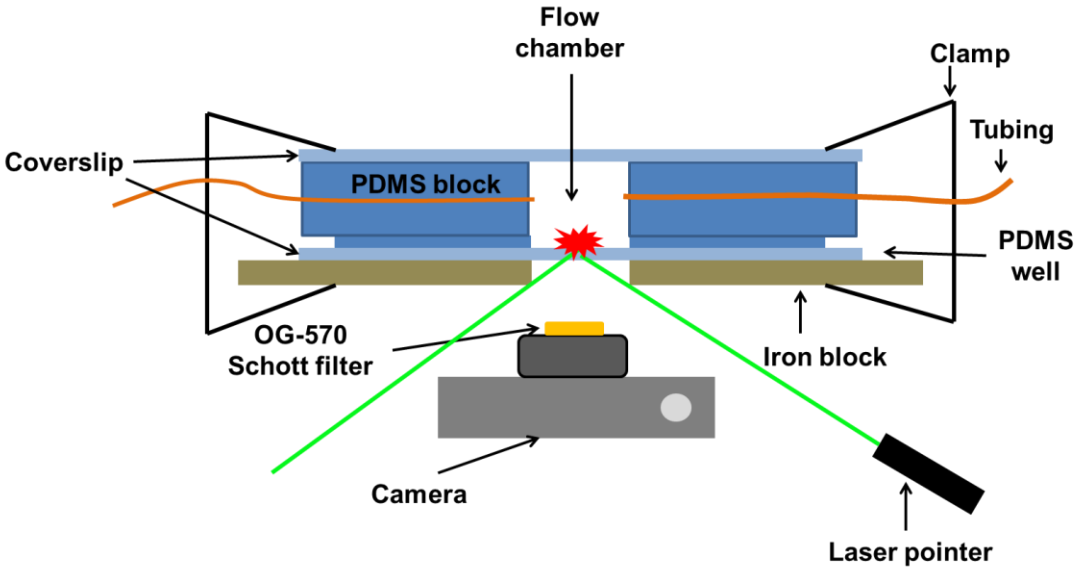

Figure 2.6. Flow Cell for Inexpensive Fluorescence Detector. The diagram shows the fabrication of the flow cell and the mounting of the flow cell in the inexpensive fluorescence detector. The inlet and outlet hole is drilled on either side of the PDMS block instead.

CHAPTER III

SENSING SMALL MOLECULES AND LIPID MEMBRANES INTERACTIONS BY LOCAL PH MODULATION*

Introduction

A great number of small drug molecules currently on the market target membrane localized proteins, such as receptors and ion channels.[28, 29] These molecules can also directly or indirectly interact with the surrounding lipid membrane,[30-33] which may lead to changes in a drug's function, properties, and availability.[34] Thus, it is important to understand the intrinsic interactions between drug molecules and lipid membranes. As most drugs are small molecules, whose properties may be altered greatly upon fluorescent labeling, it is imperative to employ label free methods to study small molecule-membrane interactions. A number of techniques have been employed to detect these interactions including UV-Vis spectroscopy,[63] nuclear magnetic resonance (NMR),[64-66] electron paramagnetic resonance (EPR),[67] quartz crystal microbalance with dissipation monitoring (QCM-D),[68] isothermal titration calorimetry (ITC),[69] vibrational spectroscopy (both infrared and Raman),[70-73] second harmonic generation (SHG) imaging,[34] ultraviolet-visible sum-frequency generation (UV-Vis SFG),[74] differential scanning calorimetry (DSC),[75, 76] and fluorescence spectroscopy based on a drug's intrinsic fluorescence.[77]

---

* Reprinted with permission from "Sensing Small Molecule Interactions with Lipid Membranes by Local pH Modulation" by Huang, D.; Zhao, T.; Xu, W.; Yang, T.; Cremer, P. S. *Anal. Chem.* [Online early access]. DOI: 10.1021/ac401955t. Published Online: Oct. 23, 2013.

The methods enumerated above differ widely in their ease of use, signal-to-noise limits, expense, and requirements for technically trained operators. For example, QCM-D is relatively easy to use, but has only modest sensitivity. Sensing based on a drug's intrinsic fluorescence may be quite useful in specific cases, but is not universally suitable because of the limited fluorescence of many candidate molecules. On the other hand, SHG and UV-Vis SFG are more universal techniques, but require more sophisticated equipment and more advanced operator training. Moreover, NMR and EPR can potentially provide detailed molecular-level information, but are of limited importance in high-throughput screening and have limited sensitivity. Raman and IR have better sensitivity, but provide less chemically-specific information and still are probably of only limited use in the development of screening assays. Perhaps the most widely accepted technique is ITC, which is often used to monitor drug molecule interactions with lipid vesicles in solution. Its sensitivity is limited by the degree of exothermicity of a given binding event and studies with ITC require highly concentrated samples.

Herein, we will describe a new technique that uses much less lipid material, has higher throughput and provides improved signal-to-noise compared with ITC. Moreover, this method works with supported lipid bilayers (SLBs),[62, 78, 79] which affords the ability to perform heterogeneous assays. This is a significant development because lipid vesicle solutions are employed in ITC in homogeneous assay formats, whereby drug molecules are constantly injected into continuously diluted samples. The advantage of heterogeneous assays with SLBs is that they can be run with a single lipid bilayer while

the adjacent buffer solution is continuously replaced.[80-85] SLBs have been widely used as model cell membranes *in vitro*,[44, 45] and can have similar lipid compositions to cellular membranes as well as maintain the same two-dimensional fluidity.[79] Additionally, for studying drug-membrane interactions, it is advantageous to employ SLBs instead of liposomes, as SLBs require far less sample volume. Moreover, they can be integrated into an on-chip platform as part of a microfluidic device.

The strategy we wished to develop for detecting small molecule-membrane interactions is based on pH modulation sensing.[25, 86, 87] In the case of lipid membranes, this involves directly conjugating a pH sensitive dye such as *ortho*-Texas Red[25] or *ortho*-rhodamine B[87] to a phosphatidylethanolamine (PE) lipid embedded within a bilayer. These two dyes have been tested to show no obvious photobleaching behavior under the experimental condition.[25, 27] Previously, we have shown that assays for target proteins can be developed when membrane-conjugated ligands are added to the membrane.[28,30] Upon binding of a target protein with a net charge, the interfacial potential is modulated, which in turn shifts the protonation state of the pH sensitive dye molecule. This strategy is extremely sensitive and can detect target protein concentrations in bulk solution with the K_d value several orders of magnitude lower than that for the corresponding ligand-receptor binding event. As such, we reasoned that it should be possible to extend this idea to small molecule-membrane interactions in a heterogeneous assay, in which QCM-D, SPR, or ITC have more difficulties due to intrinsic signal-to-noise limitations.

Herein, we demonstrate that the pH modulation approach can be exploited to monitor tetracaine-phospholipid interactions with outstanding sensitivity. Tetracaine is

an anesthetic drug with a pK_A near 8.9 (molecular structure provided in Figure 3.1).[22,88,89] Its main activity is known to involve the blocking of ion channels in cell membranes. Extensive investigations of tetracaine-membrane interactions have been made over the last several decades. This includes the anesthetic mechanism for this drug,[90, 91] its location within the lipid bilayer,[92, 93] and the influence of the ionization state of tetracaine on its binding properties.[77] It has been reported that tetracaine inserts into biomembranes in the way that the butylamino group resides inside the lipid tale group region, while the protonated dimethylamino moiety is positioned near the phosphate moiety of the lipid head group.[93]

For the current experiments, 0.5 mol% *ortho*-rhodamine B-conjugated POPE (oRB-PE) was embedded in POPC bilayers to detect tetracaine (Figure 3.1). The experiments were performed at pH 7.1, where the drug bears a positive charge in bulk solution. Also, this pH falls within the linear range of the pH titration curves while still close to physiological pH (Figure 3.2). Upon introducing the drug, a reversible decrease in the fluorescence response from oRB-PE was observed. This is consistent with the drug molecule making the interfacial potential more positively charged. By varying the drug concentration, it was possible to obtain a binding curve for the tetracaine/membrane interaction (K_d = 180 ± 47 μM). Moreover, it was found that this dissociation constant could be modulated by varying the lipid composition in the membrane.

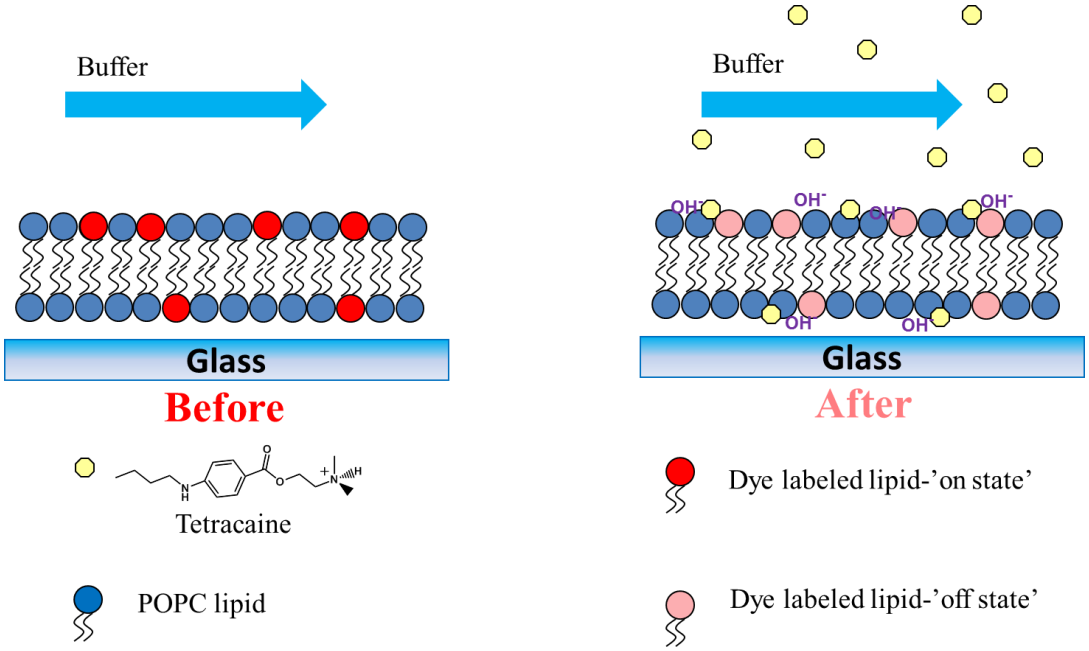

Figure 3.1. Principles of Drug-Membrane Interaction Sensing. The Schematic diagram illustrates the principles of oRB-PE acting as a reporter for drug-membrane binding. (Before) In the absence of the drug molecules, the fluorescent dyes are in the "on state", which is shown in in red. (After) Upon binding the drug molecules, the interfacial potential is increased, which recruits OH^- to the surface. As a result, the dye molecules in the lipid membrane are turned off (shown in pink).

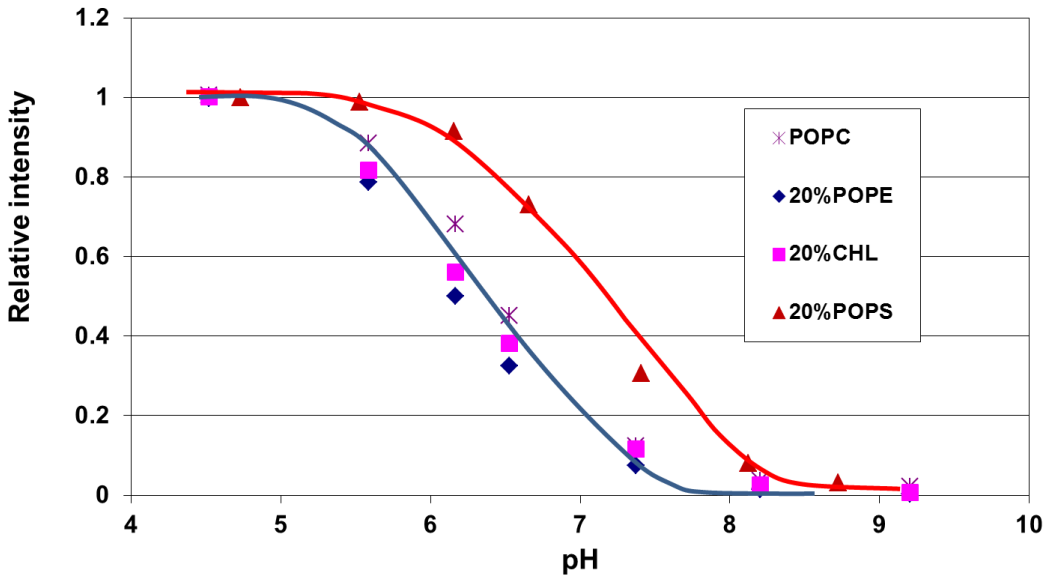

Figure 3.2. pH Titration Curves for Different Supported Lipid Bilayers. The plot shows the titration data for each selected membrane composition. The solid circles represent individual fluorescence measurements and the solid lines are guides to the data.

Tetracaine-Membrane Interaction Sensing Results and Discussion

Sensing Tetracaine-POPC Supported Bilayer Interactions. SLBs containing 99.5 mol% POPC and 0.5 mol% oRB-PE were utilized for sensing tetracaine-membrane interactions in an initial series of experiments. This work was performed with 50 mM sodium phosphate buffer at pH 7.1 ± 0.1.[87] The buffer was flowed over the patterned bilayers until fluorescence stabilization was achieved (Figure 3.3(a)). Next, tetracaine at concentrations ranging from 0-500 μM was introduced into the buffer and continuously flowed through the flow cell until the fluorescence intensity from the lipid bilayer stabilized. Images were captured every 5 minutes and stabilization took about 30 minutes at the lowest drug concentration. There are two reasons for the relatively slow response time. First, the diffusion process for tetracanine to arrive at the surface from the bulk solution takes every more time as the concentration is lowered. Since we are in the μM range in this experiment, it is not a very significant factor. On the other hand, the flow chamber has a dead volume of ~250 μL. To replace this solution once takes ~15 minutes at a flow rate of 1 mL/hour. Thus, the response time could be significantly decreased, if desired by using a smaller flow chamber. A representative image after equilibration with 500 μM tetracaine is shown in Figure 3.3(b). The individual fluorescence line scans for 8 different tetracaine concentrations are shown in Figure 3.3(c). As can be seen, the fluorescence intensity of the lipid bilayer decreased with increasing concentration of the drug molecule. At the highest concentration of tetracaine

employed, 500 μM, the fluorescence intensity decreased by more than a factor of three. By flowing out the drug molecule, the fluorescence reverted back to the starting intensity and, hence, the whole process was completely reversible over at least five cycles of introducing and removing tetracaine, which is demonstrated in Figure 3.4. This indicates tetracaine can be completely removed from the membrane. The data in Figure 3.3(c) represent a signal-to-noise ratio of ~400:1. This corresponds to a detection limit of about 3 μM at the 99% confidence level under the identical experimental and instrumental condition.

Using the data from Figure 3.3(c), the relative fluorescence intensity decrease could be plot as a function of drug molecule concentration (Figure 3.3(d)). The *y*-axis represents the relative fluorescence change ΔF, which is calculated as $(F-F_0)/F_0$, which reduces to F/F_0-1. In this equation, F is the fluorescence intensity of the bilayer as a function of tetracaine concentration in the bulk solution, whereas F_0 is the fluorescence intensity of the bilayer in pure buffer.

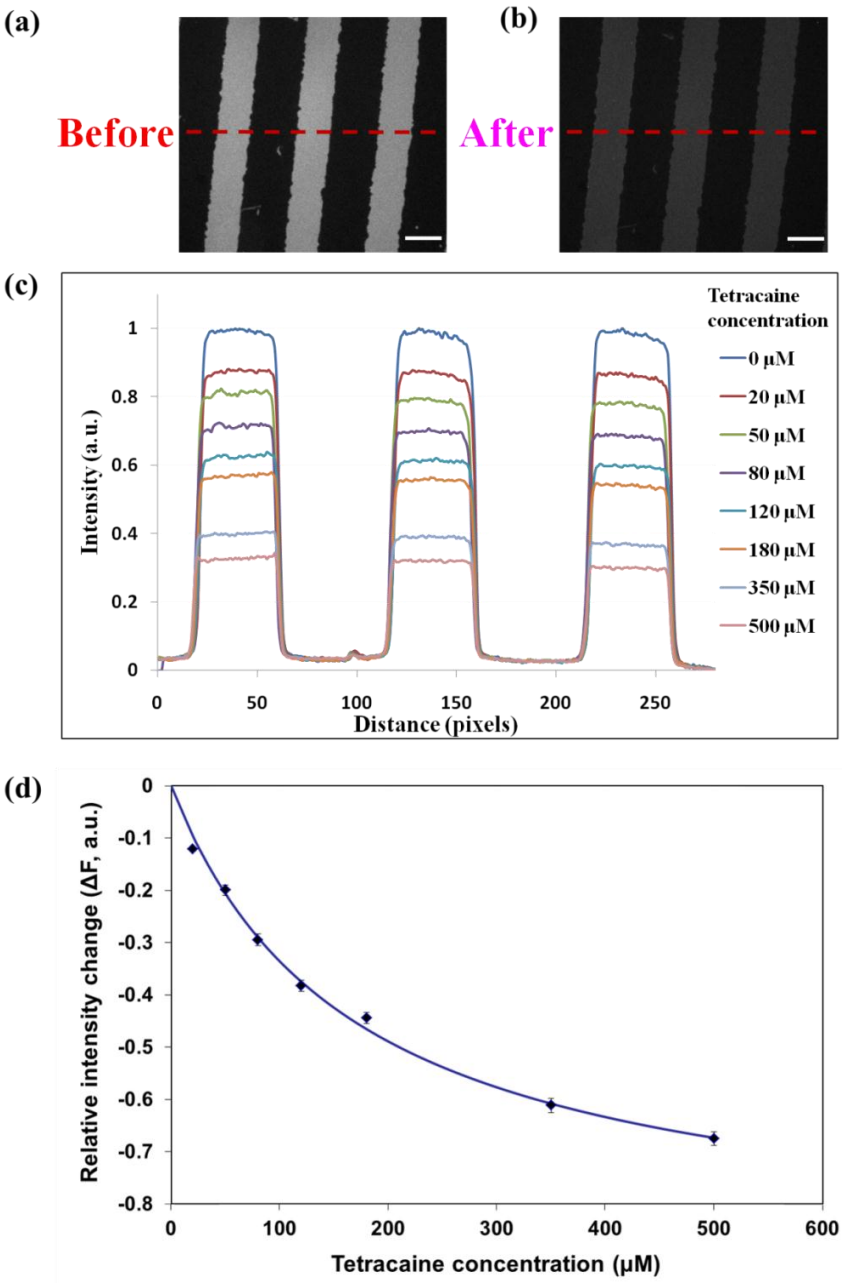

Figure 3.3. Sensing Tetracaine-POPC Bilayer Interaction. Epi-fluorescence image of a stripped bilayer pattern in a flow cell is obtained (a) before and (b) after the introduction of 500 µM tetracaine. The scale bars shown in white are 1 mm. (c) Line scan profiles for the same patterned bilayer under bulk tetracaine concentrations ranging from 0 to 500 µM. The red dash lines in (a) and (b) represent the regions used obtain the line scans. (d) Plot of the relative fluorescence intensity change vs. bulk tetracaine concentration. The blue solid line is the best fit to a Langmuir isotherm for these data points.

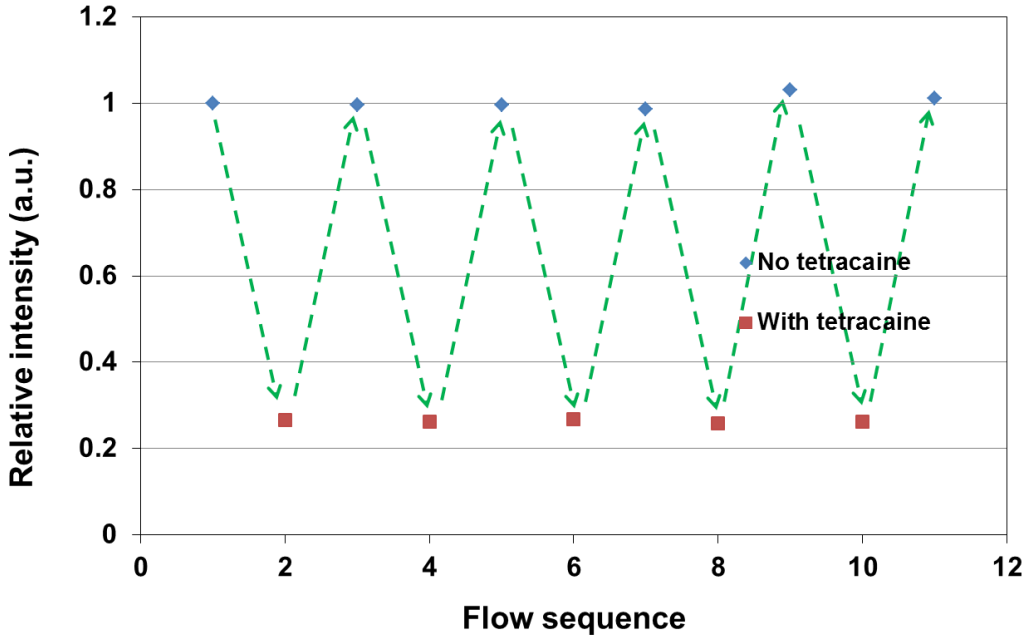

Figure 3.4. Reversibility Test for Tetracaine-POPC Bilayer Interaction Assay. The blue dots are POPC SLB flowed with 50 mM pH 7.1 phosphate buffer, while the red dots are POPC SLB flowed with 50 mM pH 7.1 phosphate buffer containing 500 µM tetracaine. The flow rate was approximately 1 ml/h. The SLB were stabilized under each condition for at least 30 min.

The data in Figure 3.3(d) can be fit to a Langmuir isotherm as shown by the blue solid line. The apparent equilibrium dissociation constant is abstracted using equation 3.1:

$$\Delta F = -a\frac{[T]}{K_d+[T]} \tag{3.1}$$

where T is the bulk concentration of tetracaine and a is a constant corresponding to the maximum relative fluorescence intensity change. The fit yields a K_d of 180 ± 47 μM, which is consistent with the literature value for this binding event found by non-linear optical measurements.[34] As a control experiment, the direct interaction of tetracaine with the dye molecule was probed in bulk solution in a QVFL-Q-10 cuvette within a QE 65000-FL Scientific Grade Spectrometer. In this case, 1 μM *ortho*-rhodamine B-conjugated biotin was placed in a 50 mM sodium phosphate buffer solution (pH 7.1 ± 0.1). Solution conditions were varied to consist of up to 1 mM tetracaine. No changes in the fluorescence intensity were noted within experimental error, even at the highest concentration of the drug molecule.

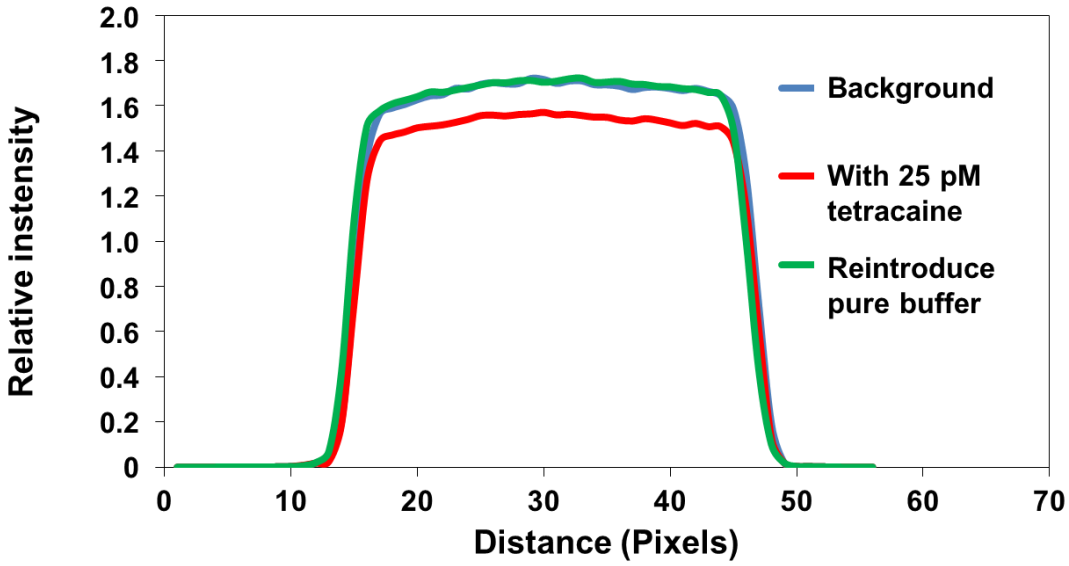

Figure 3.5. Detection Limit Assay. The plot shows the fluorescence intensity line scan of a POPC SLB under 0.5 mM sodium phosphate buffer (pH 7.1 ± 0.1) without tetracaine (blue and green) and with 25 pM tetracaine (red).

It should be noted that although the detection limit was 3 μM for the experiments in Figure 3.3, this value could easily be lowered by several orders of magnitude by simply averaging the data over the entire sample area, making multiple measurements as a function of time, or decreasing the buffer concentration by analogy with work done for protein-membrane interactions.[25, 87] For example, by utilizing a 10X objective and 0.5 mM sodium phosphate buffer solution (pH 7.1 ± 0.1), it was easily possible to detect 25 pM tetracaine (Figure 3.5) with detection limit of ~10 pM. This measurement was also completely reversible after the reintroducing of pure buffer. The reason for the improved detection limit under these conditions is the higher light gathering power of the 10X objective (NA = 0.30 vs. only NA = 0.13 for 4X object). Moreover, the decrease in the ionic strength of the solution led to an increase in the Debye length. This will, in turn, allow more distant fluorophores to be effected under otherwise similar experimental conditions as we have already shown for protein detection.[25, 27] An even lower detection limit can be achieved by further decreasing the ionic strength. It should be noted, a detection limit of ~1 pM tetracaine was achieved by working at 5 μM sodium phosphate buffer (pH 7.1 ± 0.1). However, the buffering capacity of the solution is eroded as it the buffer concentration is lowered. Therefore, there is a trade-off between the limit of detection and maintaining a stable pH value. A 5 μM buffer seems to represent a practical limit for this.

Effect of Cholesterol on Tetracaine-Bilayer Binding. In a next set of experiments, cholesterol was introduced to POPC SLBs with 0.5 mol% oRB-PE and tested for tetracaine interactions. Cholesterol is an important constituent in mammalian cells which

varies significantly in concentration in the membranes of various organelles.[94, 95] It influences cell membranes via its interactions with lipids and membrane associated proteins.[96] Herein, cholesterol concentrations were varied from 0 mol% to 45 mol%. The assays were otherwise carried out under the same conditions as those in Figure 3.3. Fluorescence modulation assays were performed with 5 different cholesterol concentrations (Figure 3.6(a)) and the values for K_d as a function of cholesterol are plotted in Figure 3.6(b). As can be seen, K_d weakened approximately three fold and did so in a linear fashion with increasing cholesterol concentration. This attenuation in the strength of the tetracaine-bilayer interaction is in agreement with previous reports. Specifically, Zhang and co-workers found that 28 mol% cholesterol in DPPC bilayers decreased the partition coefficient of tetracaine to the bilayer both below and above its phase transition temperature.[77] Nguyen et al. have shown that a decrease in tetracaine binding to SOPC, DMPC, and DPPC bilayers could be observed after incorporating 28 mol% cholesterol.[34] Both of these previous studies were, however, performed at just this single concentration of cholesterol. Our current data showing a linear weakening of the K_d value with the mol% cholesterol in a POPC bilayer is consistent with the notion that cholesterol increases the packing density of the lipids in the bilayer and leaves less room for the small molecule to insert.[7] In fact, according to Kim et al., the mean head group area per DPPC molecule should decrease linearly with increasing cholesterol concentration.[97]

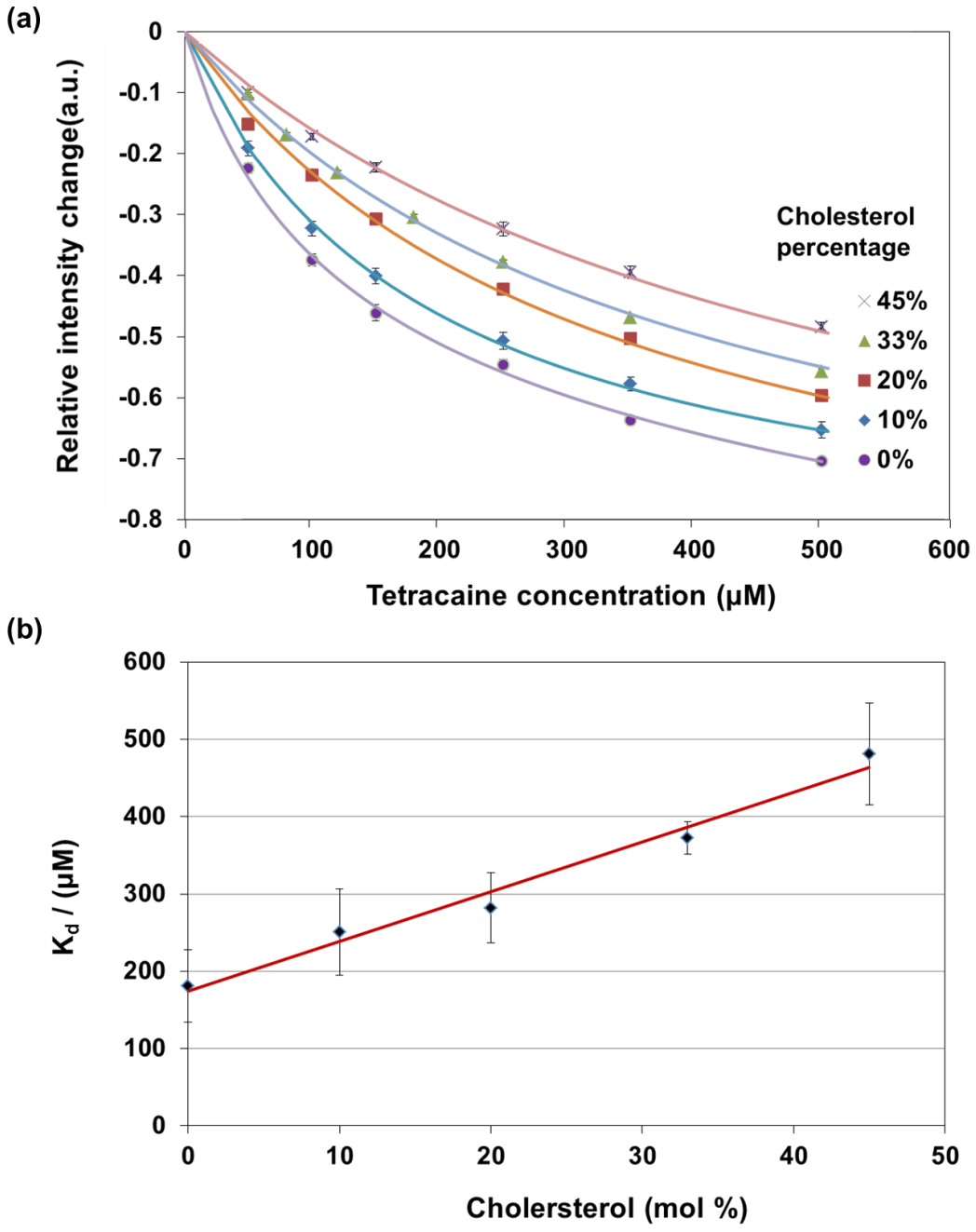

Figure 3.6. Cholesterol Influence on Tetracaine-POPC Bilayer Interaction. (a) Plots of relative fluorescence intensity change vs. bulk tetracaine concentration for five different cholesterol concentrations: 0, 10, 20, 33, and 45 mol%. The solid lines are the best fits to Langmuir isotherms. (b) A plot of K_d vs. cholesterol concentration from the data in (a). The red solid line represents the best linear fit to the data.

Effect of POPE on Tetracaine-Bilayer Binding. Phosphatidylethanolamine (PE) is composed of a glycerol moiety that is esterified with two fatty acids and a phosphate group. The negatively charged phosphate group is conjugated to a positively charged ethanolamine group, which makes the whole molecule zwitterionic at pH 7.1 ± 0.1. PE usually constitutes 20-50% of total phospholipid content in mammalian cells, which makes it the second most abundant lipid after phosphotidylcholine (PC).[98] Thus, it is important to discern the influence of PE on tetracaine/membrane interactions. For the current studies, POPE was chosen as a model PE lipid, because it has the same tale groups as POPC. It should be noted that PE is more basic than PC with pK_a = ~9.6 for the amino group.[99]

To test the influence of POPE on tetracaine-bilayer interactions, up to 20 mol% POPE was incorporated into POPC SLBs. This upper concentration limit was chosen because greater PE concentrations may impede vesicle fusion to the planar glass supports.[100] Binding curve data are provided in Figure 3.7 and the extracted apparent K_d values are plotted in Figure 3.8. As can be seen, PE had the opposite effect of cholesterol. Specifically, the K_d value for tetracaine binding tightened from 180 ± 47 μM to 124 ± 23 μM when 20 mol% POPE was added to the SLBs. Once again, the trend appeared to be linear with the added lipid component.

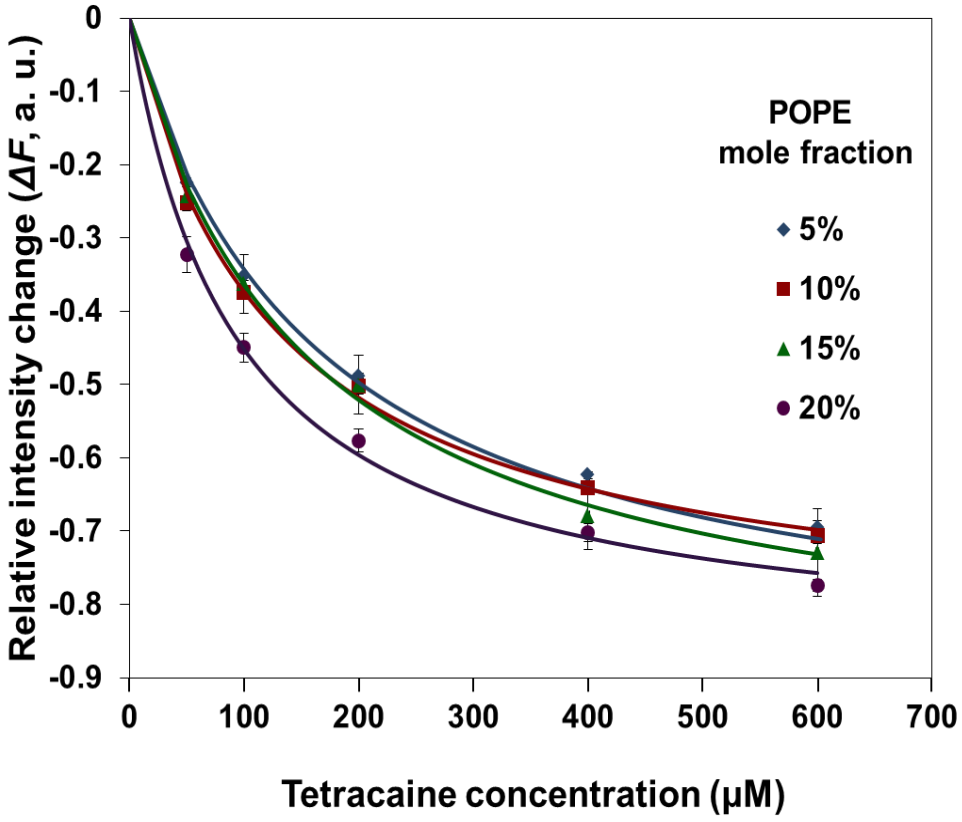

Figure 3.7. Binding Curves for POPE Bilayers. The figure shows the plots of the relative fluorescence intensity change vs. bulk tetracaine concentration from bilayers containing various concentrations of POPE. The solid lines re the best fit to Langmuir isotherms.

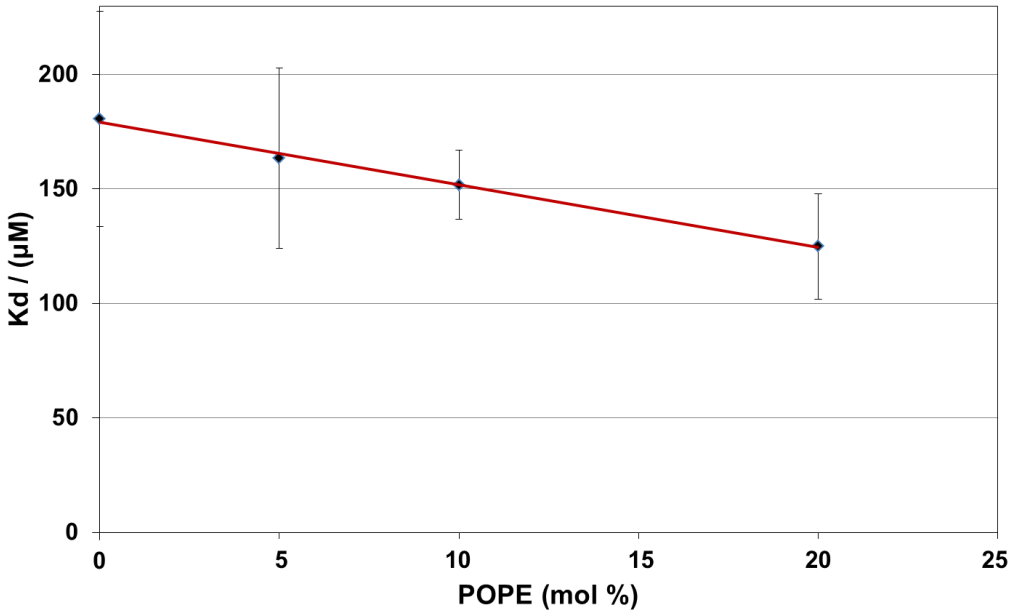

Figure 3.8. POPE Influence on Tetracaine-POPC Bilayer Interaction. The figure shows the plot of the K_d value for tetracaine vs. the POPE concentration in POPC membranes. The red solid line represents a linear fit to the data.

The linear increase of tetracaine affinity with increasing POPE concentration may attribute to hydrogen bonding between POPE lipids and tetracaine. Several studies have demonstrated the ability of PE to form hydrogen bond with various small molecules.[101-104] Herrera et al. demonstrated that there are hydrogen bonds forming between an amino acid's carboxylate group and the $R\text{-}NH_3^+$ from PE when arginine interacts with the DMPE bilayer. Moreover, the carbonyl moiety of PE lipid is able to form hydrogen bond with the guanidinium moiety of arginine.[101] Besides, Pink et al. have proposed hydrogen bond formation between PC and PE, which would need to form between either the NH_3^+ and PO_2^- or NH_3^+ and C=O.[103] By analogy, a hydrogen bond is likely to form in between the $R\text{-}NH_3^+$ group on POPE and the C=O group on tetracaine.

It has been observed that the incorporation of PE into phospholipid bilayers reduces interchain hydration while enhancing head group hydration.[105] However, because PE lipids have a relatively small and cone shaped head group, it is energetically unfavorable to have an increase in head group hydration, which makes planar bilayers unstable.[106, 107] Evidence from a *^{31}P-NMR* study has shown that tetracaine inserts into PE-containing bilayers by acting as a wedge, which helps stabilize the membrane.[108] As such, the relatively stronger affinity between tetracaine and POPE-containing bilayers may be the result of relieving the lipid packing constraints caused by the presence of POPE.

Effect of Negatively Charged Lipids on Tetracaine-Bilayer Binding. In addition to uncharged and zwitterionic components, there are also negatively charged lipids in bilayers such as phosphatidylserine (PS), phosphatidylglycerol (PG) and gangliosides. Although they are not as abundant in biological membranes as PE or cholesterol, negatively charged lipids are tightly regulated and play a key role in membrane chemistry.[109-114] Moreover, these components should interact at least electrostatically with the positively charged tetracaine.

Experiments were carried out with POPG, POPS, and GM1 using similar conditions and procedures as described above. The buffer for POPG and GM1-containing SLBs was 50 mM sodium phosphate (pH 7.1 $\pm$ 0.1). While the buffer with POPS contained 0.8 mM EDTA due to the potential quenching ability of trace concentrations of divalent metal ions such as Cu^{2+}.[115] The associated binding curve data are provided in Figure 3.9. The apparent dissociation constant for tetracaine as a function of each negatively charged lipid components are provided in Figure 3.10. It should be noted that data at 30 mol% is only provided for POPG and POPS as vesicles containing 30 mol% GM1 would have difficulty in forming supported bilayers.

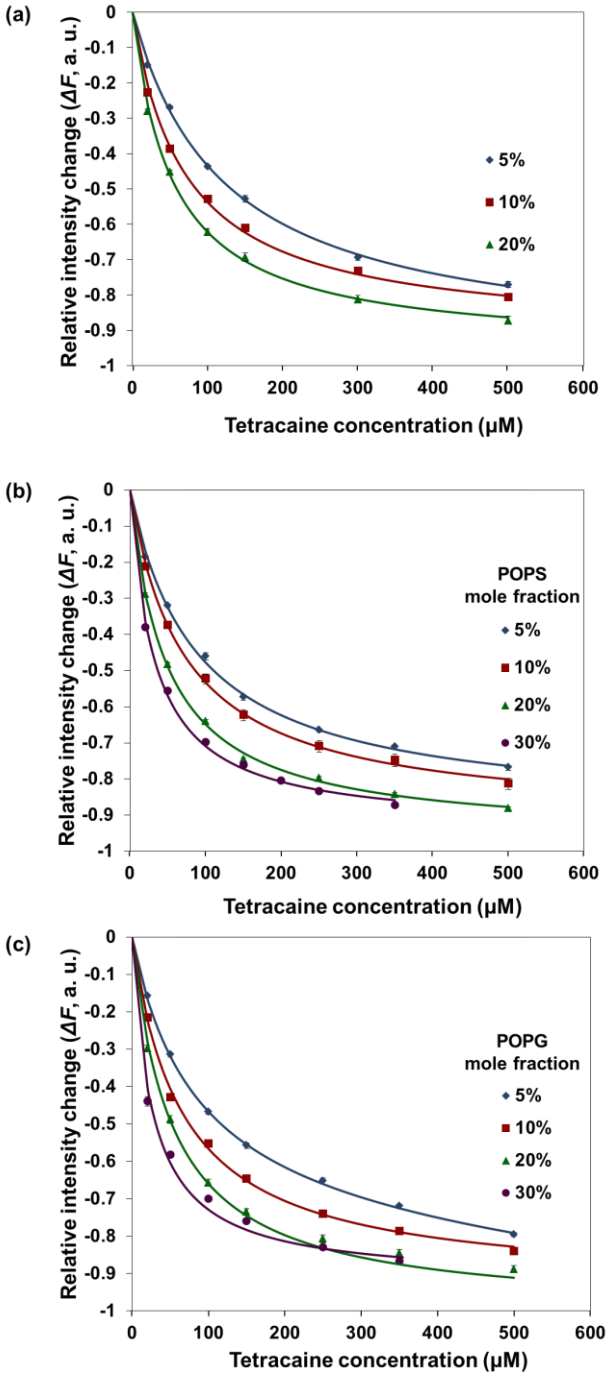

Figure 3.9. Binding Curves for Negatively Charged Lipids Contained Bilayers. The figures show the plots of the relative fluorescence intensity change vs. bulk tetracaine concentration from bilayers containing various concentrations of negative charged lipids: (a) GM1 containing bilayers, (b) POPS containing bilayers, and (c) POPG containing bilayers. The solid lines are the best fits to Langmuir isotherms.

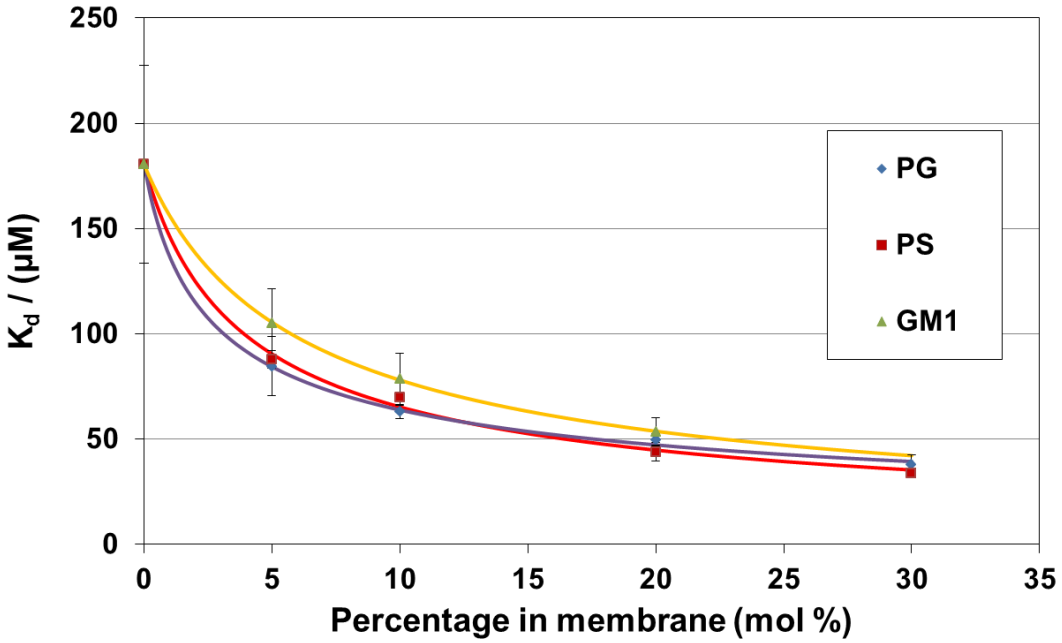

Figure 3.10. Influence of Negative Charge on Tetracaine-POPC Bilayer Interaction. The figure shows the plots of the K_d values for tetracaine vs. the mol% of negatively charged lipids for PG (blue diamonds), PS (red square), and ganglioside GM1 (green triangle). The solid curves represent the best curve fit to the data.

As can be seen from Figure 3.10, the influence of POPS, POPG, and GM1 on the K_d values are essentially identical. Thus, the effect should be simply electrostatic rather than chemically specific. Indeed, the incorporation of any of these three molecules into the bilayer will make the surface potential more negative.[116] This in turn will enhance the electrostatic interactions between the bilayer and the positively charged tetracaine molecules. Moreover, the presence of negatively charged lipids leads to a tightening of the dissociation constant only at lower concentrations of the negatively charged lipid, while this effect flattens out as the concentration is increased further. This finding is consistent with the idea that the surface potential decreases non-linearly as additional negatively charged lipids are introduced into the membrane.[116] The overall effect is to tighten the dissociation constant by approximately a factor of six when 30 mol% of a given negatively charged lipid is present (Figure 3.10).

Comparison with ITC. As noted in the introduction, a variety of methods have been employed to investigate the interactions of membranes with small molecules.[63-77] As ITC is probably the most commonly employed of these techniques, we wished to benchmark the current pH modulation results against it. To do this, ITC measurements were performed with a MicroCal Auto-iTC200 (Pittsburgh, Pennsylvania) using similar tetracaine-POPC binding conditions described in Figure 3.3. However, since measurements could not be made with supported bilayers, 100 nm diameter POPC vesicles (0.76 mg/ml) in 50 mM sodium phosphate buffer (pH 7.1 ± 0.1) were used instead. In order to obtain a binding curve, 1.5 μL of 10 mM tetracaine aliquots were introduced into 370 μL of the vesicle solution in 25 separate injections. A K_d value of

126 ± 65 μM was found for this interaction and the detection limit was ~1 μM. Experiments were also run with POPC vesicles containing 0.5 mol% oRB-PE. In this case we found K_d = 103 ± 53 μM. The raw ITC data and curve fits are provided in Figure 3.11. Within experimental error, both of these measurements are the same and agree well with the data from Figure 3.3 where a value of 180 ± 47 μM for K_d was found. Such ITC measurements serve as an additional control to verify that adding 0.5 mol% oRB-PE as a probe in the pH modulation assays had little if any effect on the experiment. It should be noted that there could be a small difference in the K_d values between the ITC and pH modulation experiments since the former was done with vesicles and, thus, have curved surfaces, while the supported membranes are essentially flat. Apparently, any binding differences caused by this degree of curvature do not lead to significant differences within experimental error.

There are significant advantages of making drug-membrane interaction measurements by the pH modulation technique compared with ITC. One essential factor is the relatively small sample amount required in the former case. In fact, in order to obtain an acceptable signal from ITC, 400 μL of 0.76 mg/ml vesicle solution must be prepared. Moreover, 1.5 μL of highly concentrated (10 mM) tetracaine aliquots were introduced into the vesicle solution in 25 separate injections. By comparison, the amount of lipid material required in the pH modulation setup was several orders of magnitudes less. It should be noted that the pH modulation experiments can also be run in microfluidic channels, where only a few microliters of bulk sample would be flowed, although that was not done here. Smaller lipid and drug sample volumes would represent

a significant advantage when exploring the interactions of expensive or rare drug molecules with membranes. Secondly, the pH modulation assay can be run under conditions where the detection limit of the assays outstrips ITC by at least 4 or 5 orders of magnitude (Figure 3.5). Thirdly, the cost of a typical ITC instrument is over $100,000, whereas fluorescence measurements can be made with a setup costing much less than this. Finally, the current fluorescence-based technique has the potential for easy multiplexing by employing patterned bilayer membranes to explore multiple membrane interactions at once.[53, 117] In fact, dozens, if not hundreds of interactions could be explored simultaneously. Such multiplexing advantages would be much more difficult to be realized by ITC measurements.

It should be noted that there are also inherent advantages of ITC. For example, this technique directly measures heat transfer, which affords the most straightforward way to obtain ΔH values for the drug-membrane interactions. One could also image circumstances under which a particular drug might directly interact with the dye molecule employed as the probe in the pH modulation sensing assay. Finally, both methods provide thermodynamic information and can thus benefit from complementary spectroscopy measurements such as FTIR, Raman, or NMR to provide molecular level details concerning drug-membrane interactions.

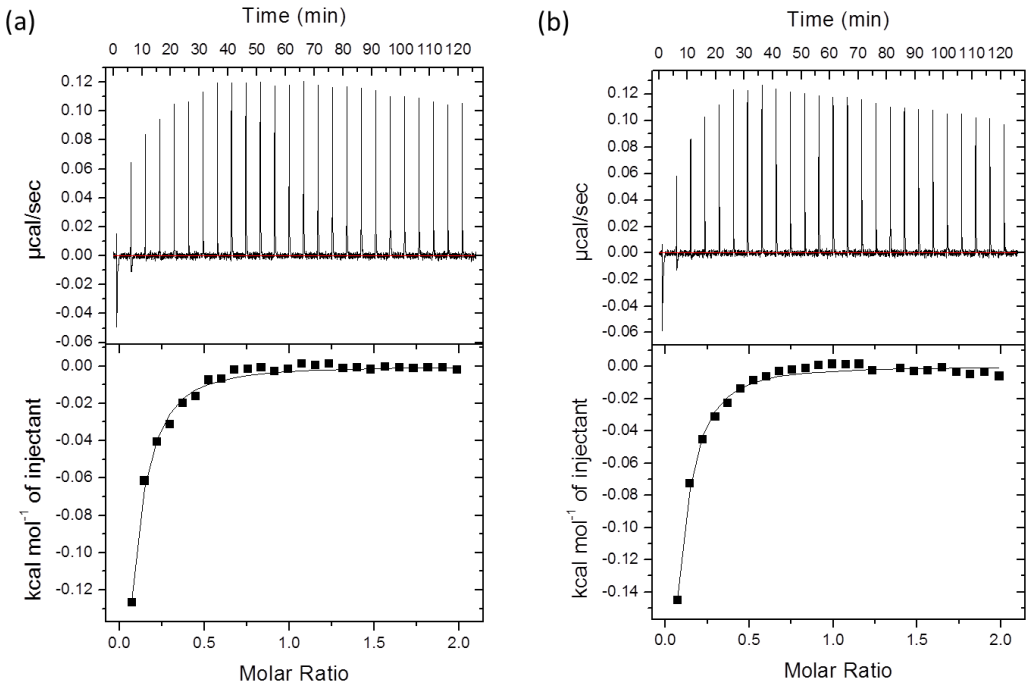

Figure 3.11. ITC Data for Tetracaine-POPC Bilayer Interaction. ITC data for (a) pure POPC vesicles and (b) POPC vesicles containing 0.5 mol% oRB-PE are shown in the graphs above. The top graphs show individual heat spikes as sample injections are made. The bottom graphs are the plots of the evolved heat vs. the molar ratio of tetracaine introduced into solutions containing POPC vesicles. And the solid lines are the best nonlinear regression fits to the data and the extracted K_d values are provided in the main text.

Conclusions

As demonstrated above, our pH modulation sensor platform can be employed to measure K_d values for the interactions of tetracaine with phospholipid membranes, which could be easily applied to study other drug molecules such as ibuprofen, aspirin, and saxagliptin.[118-120] Drug-membrane binding should arise largely from van der Waals, hydrophobic, packing, hydrogen bonding, and electrostatic interactions.[77, 93, 101] The K_d value measured for the interaction of tetracaine with supported POPC bilayers was 180 ± 47 μM. This value could be modestly weakened by adding cholesterol to the membrane (K_d = 350 μM with 33 mol% cholesterol) or modestly tightened by adding POPE or negatively charged lipids to the membrane (K_d = 35 μM with 30 mol% DOPG). Each set of measurements could be made within a few minutes. Also, the surface area covered by the lipid bilayer involved less than 10^{15} lipid molecules, since the surface coverage inside the flow device was under 1 cm^2. This platform offers a facile and rapid method for the detection of interactions between drug molecules and lipid bilayers, especially when compared with ITC. Thus, it may be developed into a rapid screening assay and used in a multiplexed format to detect interactions with many different types of lipid membranes simultaneously.

CHAPTER IV

MONITORING PROTEIN-SMALL MOLECULE INTERACTIONS BY LOCAL PH MODULATION*

Introduction

Measurements of the affinity of biomolecular interactions, such as protein-protein binding, protein-small molecule binding, and protein-ion binding not only provide insight into basic cellular processes but can also facilitate the development of therapeutics and serve as the basis for many diagnostic techniques.[35] To date, numerous efforts have been made to monitor such ligand-receptor interactions. One potential drawback is that the devices associated with these techniques can be bulky, insensitive, and/or difficult to use. For example, calorimetric methods, such as isothermal titration calorimetry (ITC),[121-123] directly measure the heat associated with a given binding process. However, this method has relatively low sensitivity and usually requires large sample volumes. Moreover, it cannot be utilized if binding causes only very modest enthalpic changes. Interfacial methods, such as Surface Plasmon Resonance,[124, 125] microcantilever sensing,[126] and nanowire sensing[127] permit detection down to the pM level and sometimes below it. Nevertheless, the requirement of immobilizing biomolecules onto surfaces can potentially cause problems. For example, the receptor sites on a protein might face the surface, inhibiting the binding process. Also, surface

---

* Part of the data reported in this chapter is reprinted with permission from *Biosens. Bioelectron.*, 38, Huang, D.; Robison, A. D.; Liu, Y.; Cremer, P. S., "Monitoring protein–small molecule interactions by local pH modulation", 74-78, Copyright 2012, with permission from Elsevier.

immobilization may influence the conformation and activity of the immobilized protein via partial or complete denaturation.[128]

Recently, Bornhop et al. (2007) developed Back-Scattering Interferometry (BSI) to study biomolecular interactions in bulk solution.[35] This method affords label-free ligand-receptor measurements with good sensitivity. It operates by exploiting the fringe patterns which are generated when a laser beam is shined onto a microfluidic channel in a direction perpendicular to the long axis of the channel. Shifts in the fringes arise when the refractive index of the solution inside the channel is changed. These shifts can be interpreted in terms of ligand-receptor binding with the aid of appropriate software.

Despite elegant advances such as BSI, there remains a pressing need to develop simple fluorescence-based techniques which can operate in bulk aqueous media. Indeed, fluorescence techniques can be sensitive down to the single molecule level[25, 129, 130] and are readily compatible with 96, 384, and 1536-well plate screening platforms.[131-133] Moreover, fluorescence assays are highly portable and can be used in conjunction with simple battery-operated, hand-held devices.[134] Efforts have been made to utilize fluorescence resonance energy transfer (FRET) techniques to study protein-ligand interactions or sense protein substrates.[135, 136] However, in order to obtain a FRET signal, two specially selected fluorescent dyes are required, one donor fluorophore and one acceptor fluorophore. These must be labeled on specific sites of the biomolecules,[137, 138] which can decrease the simplicity of such an approach.

Herein, we utilize a simple fluorescence-based biosensor assay which exploits a pH-sensitive fluorescent dye. The dye, 5-(and-6)-carboxyfluorescein, is strongly

fluorescent at high pH values and less fluorescent at low pH. Indeed, this dye is sensitive to any factors that can influence the local chemical environment, such as changes in the local dielectric constant or local electric field. The physical principle for this method is based on the idea that the pH sensitive probe can be placed in proximity to a protein binding pocket by conjugation to free lysine residues via succinimidyl ester-linkages. The apparent pKa of the dye will be modulated when charged ligands bind or through rearrangements due to allosteric effects. A schematic illustration of this concept is shown in Figure 4.1. In the example, a capture protein (shown in orange) is conjugated with fluorescein dyes. These fluorophores initially have relatively strong fluorescence, which decreases upon the binding of a target ligand (shown in purple). In this rendition, the platform is a "turn off" sensor. This can be the case if the target ligand is negatively charged at the operating pH. It will recruit hydronium ions around the capture protein environment and consequently help protonate the fluorescein probe. Alternatively, if the target ligand induces a conformational change in the protein upon the binding event, this may also influence the local chemical environment and thus modulate the intensity of the dye.

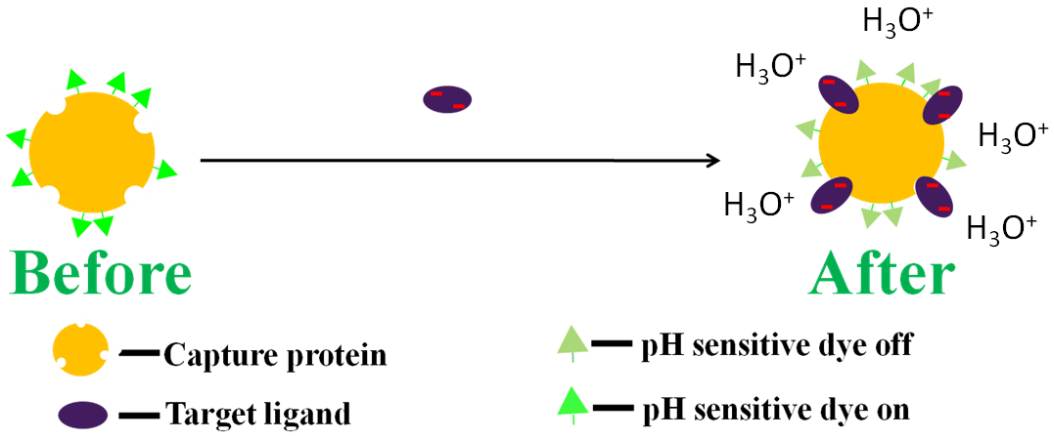

Figure 4.1. Principles of Protein-Small Molecule Interaction Sensing. (Before) In the absence of the target protein, the dye molecules conjugated to the capture protein are in the "on state". (After) Upon binding the target ligand, the negatively charged target ligand will recruit hydronium ions and decrease the local pH around the protein. As a result, the dye molecules on the capture protein are turned off.

In order for the present method to be effective, the pH sensitivity of the fluorescent probe should fall within the region of interest for measuring ligand-receptor interaction. One simple choice is 5- (and 6-) carboxyfluorescein, which has its largest fluorescence variation between pH 6.0 and pH 7.4.[139] As the dye molecule is deprotonated, its fluorescence is "turned on". Thus, this dye is an excellent reporter candidate for many biomolecular interaction assays.

Herein, we demonstrate the use of fluorescein as a local pH sensor on proteins for monitoring the interaction of proteins, small molecules, and ions, specifically observing Staphylococcal aureus Protein A (rSPA) with human IgG, thiamin monophosphate (ThMP) with thiamin binding protein A (TbpA), and Ca^{2+} with calmodulin (CaM). This platform is quite versatile and appears to be generically useful for monitoring protein-ion and protein-small molecule interactions.

Protein-Small Molecule Interaction Sensing Results and Discussion

Titration Curves for Fluorescein-labeled Proteins. In the first set of experiments, titration curves of fluorescence intensity vs. solution pH were obtained for fluorescein conjugated to TbpA and CaM. The experiments were performed by using solutions of varying pH ranging from acidic to basic. Fluorescence spectra obtained at multiple pH values are provided in Figure 4.2. As expected, the conjugated dye molecules showed higher florescence intensity at more basic pH values and lower intensity at relatively acidic pH. The titration curves were not strongly influenced by the specific protein to which the dyes were attached. The apparent pK_As were 7.0 ± 0.1, 6.5 ± 0.1, 6.4 ± 0.1, and 6.4 ± 0.1 for rSPA, IgG, TbpA and CaM, respectively.

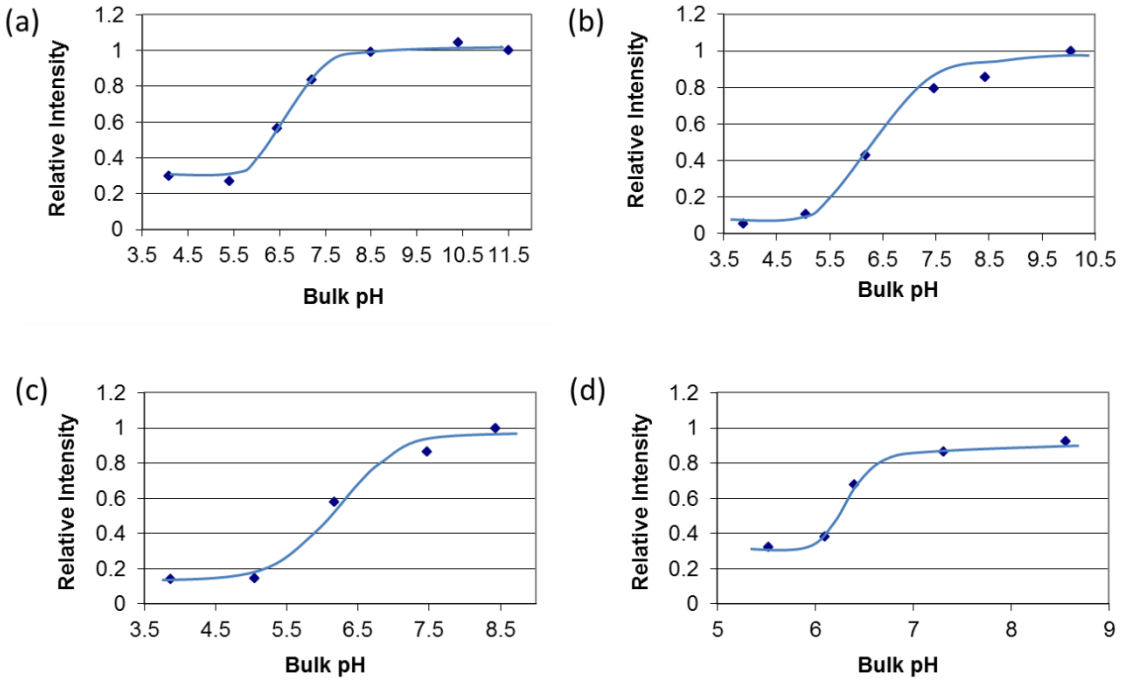

Figure 4.2. pH Titration Curves for Labeled Proteins. Single measurements of relative fluorescence intensity of 5(6)-FAM as a function of pH for different proteins are shown in the graphs above. (a) rSPA, (b) IgG, (c) TbpA, and (d) CaM. The blue lines represent guides to the eye for the titration curves.

Binding Curves for rSPA and IgG. The FC region of IgG molecules binds to rSPA in a trivalent fashion. Human and rabbit IgGs have been reported to bind with avidities ranging from K_d = 0.016 nM to 161.3 nM.[140-142] Upon rSPA-IgG binding, the fluorescence intensity increases if 5(6)-FAM was labeled on rSPA and decreases if 5(6)-FAM was labeled on IgG, as shown in Figure 4.3. This is because the pIs of rSPA and IgG are 5.1[143] and 7.2 – 8.6[144], respectively, which results in increasing the local hydronium ion activity around rSPA and decreasing it on IgG after binding.

For the 5(6)-FAM labeled rSPA, the experiment was conducted at pH 7.08, which is located in the linear range of the 5(6)-FAM titration shown in Figure 4.2(a). A concentration of 4.7 mg/mL IgG in PBS buffer was gradually added to the cuvette. This should initially result in mostly monovalent binding while progressing towards multivalent binding with increasing IgG concentration. The binding curve shown in Figure 4.4(a) could be fit by a Langmuir isotherm equation (4.1):

$$[\mathrm{IgG}]_0 = \mathrm{k} \times \delta\mathrm{F} + \frac{\mathrm{K_D} \times \mathrm{k} \times \delta\mathrm{F}}{[\mathrm{P_{rSPA}}]_o - \mathrm{k} \times \delta\mathrm{F}} \tag{4.1}$$

where $[\mathrm{IgG}]_o$ denotes the IgG concentration added, $[\mathrm{P_{rSPA}}]_o$ is the total concentration of the binding pocket on rSPA, which should be three times of the initial concentration of rSPA. K_D is the dissociation constant, δF is the relative fluorescence change $|1\text{-}F/F_0|$, where F and F_0 indicate the integrated average fluorescence intensity from 520 nm to 530nm. Also, k is a constant that describes the relationship of the fluorescence change to the concentration of substrate bound protein. The K_D value extracted from this model is 38.2 nM, which corresponds well with literature values.[141]

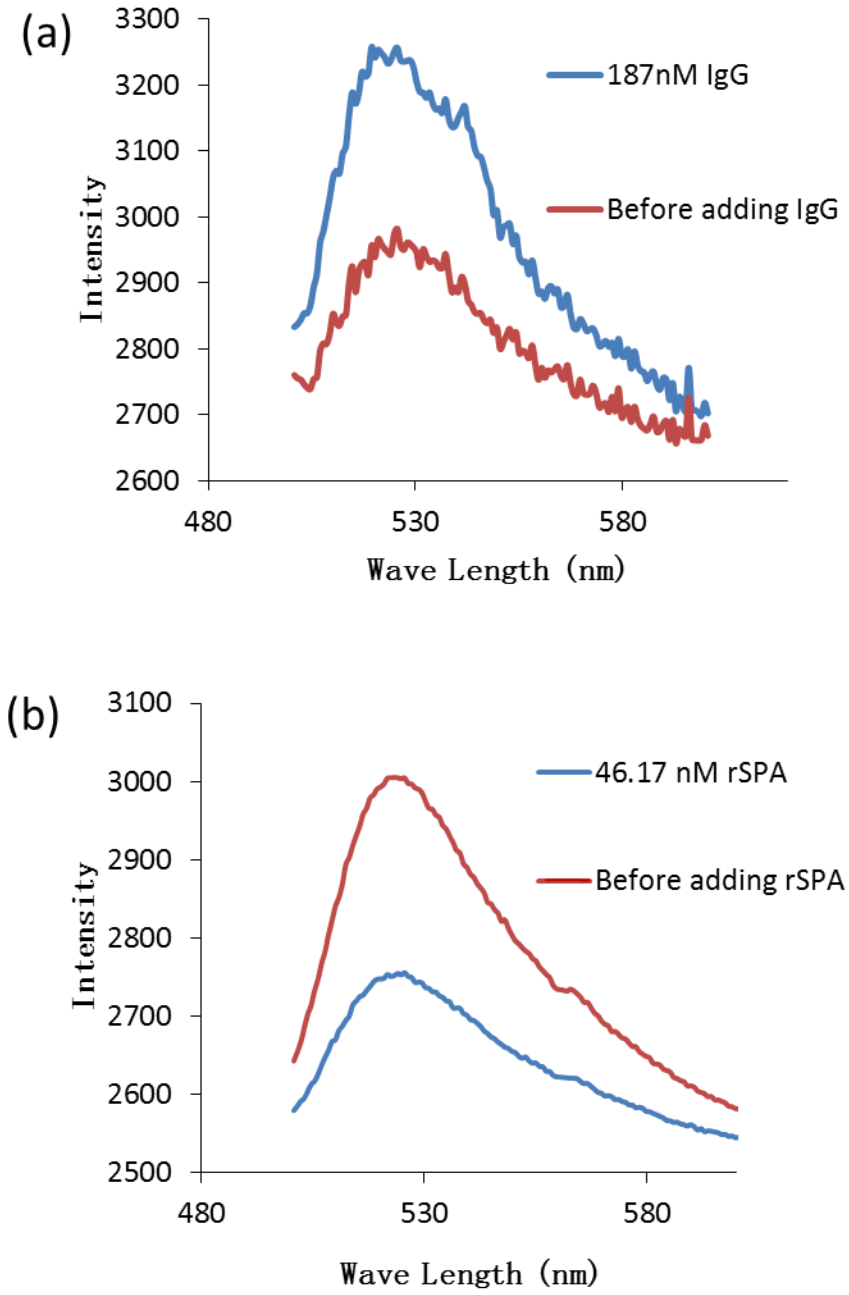

Figure 4.3. rSPA-IgG Binding Induced Fluorescence Intensity Change. (a) The fluorescence increases after adding IgG to 5(6)-FAM labeled rSPA. (b) The fluorescence decreases after adding rSPA to 5(6)-FAM labeled IgG. The difference in signal-to-noise ratios stems from the different total number of fluorophores present in the system when rSPA vs. IgG is labeled.

It should be noted that this equation differs from a standard Langmuir isotherm made with a surface containing immobilized receptor sites in contact with a bulk liquid. That is because the liquid can typically be flowed over the surface continuously until equilibrium is achieved. By contrast, in bulk solution one has a fixed number of binding pockets of rSPA proteins and these are titrated with IgG. As such, only the added amount of IgG is controlled and some of these molecules are bound while the rest are unbound. In this case, it is assumed that the fluorescence change should be directly related to the formation of the P_{rSPA} -IgG complex:

$$[\mathrm{P_{rSPA}} - \mathrm{IgG}] = \mathrm{k} \times \delta\mathrm{F} \tag{4.2}$$

Here [] denotes concentration, k is a constant representing the intrinsic relationship between the relative fluorescence change and the P_{rSPA} -IgG complex concentration. According to the definition of the dissociation constant, one can write:

$$[\mathrm{P_{rSPA}} - \mathrm{IgG}] = ([P_{rSPA}]_0 - [\mathrm{P_{rSPA}} - \mathrm{IgG}])([\mathrm{IgG}]_o - [\mathrm{P_{rSPA}} - \mathrm{IgG}])/\mathrm{K_d} \tag{4.3}$$

where $[]_o$ denotes the initial concentration or the added concentration. Combining equation (4.1) and equation (4.2) generates an equation (4.1) describing the relation of relative fluorescence intensity change and IgG concentration.

For the 5(6)-FAM labeled IgG, the assay was run at pH 6.5, which is at the center of the slope shown in Figure 4.3(b). Here the binding process will decrease the fluorescence intensity. A concentration of 0.5 mg/ml rSPA in PBS buffer was gradually added to the cuvette. This should initially result in multivalent binding before becoming monovalent at higher IgG concentrations. In contrast to the assay described above,

labeling the IgG did not result in a binding curve that could be fit by a simple Langmuir isotherm (Figure 4.4(b)). Instead, the data were fit with a Hill plot equation (4.4):

$$[\mathrm{rSPA}]_o = \frac{1}{3} \times k \times \delta F \times \frac{K_D + ([IgG]_o - k \times \delta F)^n}{([IgG]_o - k \times \delta F)^n} \quad (4.4)$$

The K_D value extracted was 1.77 nM, which also falls into the range of reported rSPA-IgG dissociation constants. The Hill coefficient *n* was 0.32, which indicated an anti-cooperative binding process.

Binding Curve for TbpA and ThMP. TbpA is the thiamin periplasmic-binding protein from *E. coli*,[145] which has been shown to bind ThMP with modestly high affinity, having a reported K_d around 2.3 nM.[146] The acidic phosphate group on the ThMP molecule brings down the local pH around the binding site of TbpA, thus making the binding of ThMP to TbpA observable via the fluorescence intensity decrease of dye-labeled TbpA. The assay pH was chosen to be 6.5, which is located just above the middle of the slope in Figure 4.2(c). TbpA and ThMP bind in a 1 to 1 ratio and a Langmuir isotherm could be employed to fit the data for the titration curve in Figure 4.4(c):

$$[\mathrm{ThMP}]_o = k \times \delta F + \frac{K_D \times k \times \delta F}{[\mathrm{TbpA}]_o - k \times \delta F} \quad (4.5)$$

The extracted dissociation constant of 3.2 ± 0.7 nM matches well with the literature value and the detection limit for ThMP is 2.1 nM. This assay provides direct evidence that the pH modulation technique is capable of following small molecule-protein binding events.

Binding Curve for CaM and Ca^{2+}. CaM, the ubiquitous Ca^{2+} binding protein, was chosen to demonstrate the ability of this method to follow protein-ion interactions. It is known that this protein can bind to and regulate a multitude of different protein targets.[35, 147] Most studies have suggested that CaM contains either multiple classes of binding sites for Ca^{2+} or negative cooperativity.[148-150] Literature K_d values for CaM-Ca^{2+} binding vary from 1 to 10 μM.[35, 151] In the current assay, the operating pH was 6.8, which is at the top of the linear range of the titration curve (Figure 4.2(d)). Interestingly, the binding of Ca^{2+} to CaM leads to a decrease in fluorescence signal, which indicates that the charge on the cation is not the dominant factor in changing the fluorescence response of the dye. CaM contains eight lysine residues, three of which are located within Ca^{2+} binding domains and one of which is C-terminally located. This C-terminal lysine is most likely to be labeled by the dye, and will experience a large conformational change based upon crystal structure analysis,[152] which results in a decrease in fluorescence intensity. The binding curve is shown in Figure 4.4(d). Note that EGTA is added to the buffer to help maintain the free Ca^{2+} concentration at a constant level.[153] The data are modeled using a Langmuir isotherm fit equation (4.6):

$$\text{Bound Sites} = \frac{[Ca^{2+}]}{K_d + [Ca^{2+}]} \tag{4.6}$$

Next, the relative fluorescence change from this binding process can be designated as δF. A constant, k, is needed to relate to CaM-Ca^{2+} complex formation. From these, an equation describing the relationship between the relative fluorescence intensity change and Ca^{2+} concentration can be written as:

$$\delta F = \frac{[Ca^{2+}]}{K_d + [Ca^{2+}]} \times \frac{1}{k} \quad (4.7)$$

The abstracted equilibrium dissociation constant was 1.1 ± 0.07 μM and the detection limit for Ca^{2+} was 0.16 μM.

The dissociation constant values measured for the two processes described above along with literature values are summarized in Table 4.1.

Table 4.1. Dissociation Constants for Protein-Small Molecule Interaction.

Binding partners	Measured K_d Values	Literature K_d Values	Detection method of published data
Protein A(FAM) - IgG	38.2 nM	0.16–160 nM	Acoustic waveguide[141] and others[140, 142]
IgG(FAM) – Protein A	1.77 nM	0.16–160 nM	Acoustic waveguide[141] and others[140, 142]
TbpA(FAM) – ThMP	3.2 nM	2.3nM	Intrinsic protein fluorescence measurement[146]
CaM(FAM) – Calcium	1.1 μM	1–10 μM	Equilibrium and flow dialysis[151]

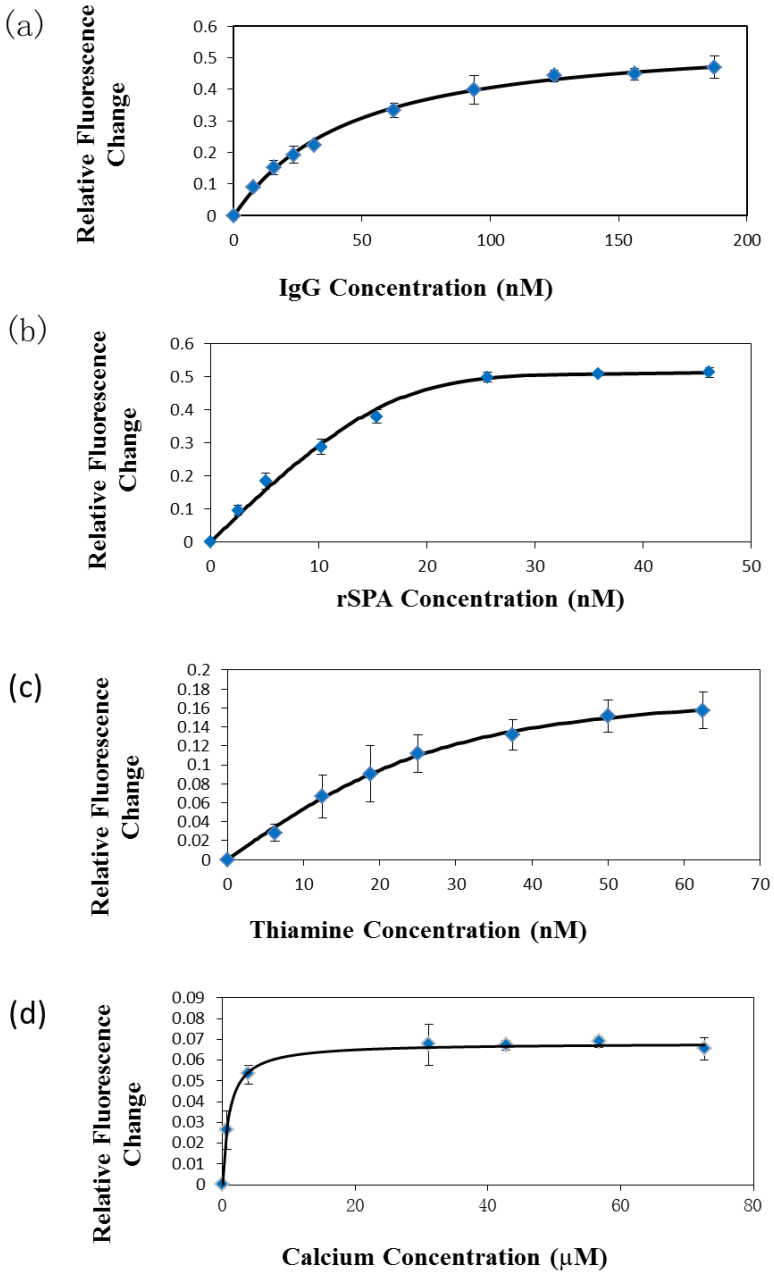

Figure 4.4. Binding Curves for Protein-Small Molecule Interaction. Plots of the relative fluorescence intensity change ($|1\text{-}F/F_0|$) vs. substrate concentration for two labeled protein-substrate binding systems are shown in the figure. The solid curves through the data are the best fits to equations. 4.1, 4.4, 4.5 and 4.7, respectively. (a) The plot for the 5(6)-FAM labeled rSPA/IgG pair. (b) The plot for the 5(6)-FAM labeled IgG/rSPA pair. (c) The plot for the 5(6)-FAM labeled TbpA/ThMP pair. (d) The plot for the 5(6)-FAM labeled CaM/Ca^{2+} pair.

Conclusions

We have developed a novel pH dependent assay for monitoring protein/substrate binding in bulk solution. This method is quite general as the assay can be employed for protein/protein, protein/small molecule, and protein/ion binding in a similar fashion. The anticipated magnitude of the relative fluorescence intensity change decreases as one move from large entities such as proteins to small molecules and ions. For the rSPA/IgG interaction assay, the maximum relative fluorescence change was around 50 percent. This is because proteins are larger species with multiple charges on them, which will strongly influence local pH after binding. However, for the TbpA/ThMP assay, because ThMP is a small molecule with fewer charges on it, the maximum relative fluorescence change is only around 16 percent. Finally, for the CaM/Ca^{2+} assay, Ca^{2+} ions are supposed to recruit hydronium ions which should increase the local pH and turn on the fluorescence. However, the conformation-induced local pH change induces a decrease in fluorescence, which ultimately dominates the signal. These competing effects result in an apparent relative fluorescence change that is even smaller.

As long as ligand-receptor binding sites are located within the Debye length of the pH sensitive dye, the conjugated fluorophore will be sensitive to the binding of a ligand molecule. Under physiological conditions (about 100 mM salt), the Debye length is typically on the order of 1-2 nm. Therefore, each conjugated dye will work as a local sensor that investigates the pH around a few square nanometers of protein surface area. The binding of a ligand to the binding pocket of a protein will modulate the protonation of D, E, K, R, and H residues as well as cause the protein to undergo a conformational

change. Both of the effects will ultimately modulate the local electric fields in the vicinity of the fluorescent probe. In our assay, the binding of rSPA to FAM-labeled IgG decreases the fluorescence intensity, while the binding of IgG to FAM-labeled rSPA increases the fluorescence intensity. This is expected in accordance with pI values of those proteins, though there may well be additional effects due to binding-induced conformational change. However, for the CaM/calcium pair, the observed signal is certainly due to a conformational change of CaM upon calcium binding because a decrease in fluorescence is observed rather than an increase, considering that the binding of Ca^{2+} should increase the local pH on electrostatic grounds. Therefore, local changes near the dye molecule due to allosteric effects apparently override this change.

A key advantage of the pH modulation technique is its ability to separately monitor both entities in a multivalent binding reaction by simply reversing the labeling on the binding pair. For rSPA/IgG, it was possible to label rSPA and obtain a saturation binding curve that followed simple Langmuir isotherm behavior. On the other hand, labeling the IgG led to non-Langmuirian behavior with a Hill coefficient of 0.32. This value represented a strong negative cooperativity effect. Such negative cooperative may be due to the steric hindrance that occurs when multiple IgG molecules bind to the same rSPA. Indeed, the IgG is much larger than rSPA. The different results when applying the assay in one direction, i.e. adding the IgG to the rSPA, as opposed to the reverse may be due to the multivalent binding behavior of IgG-rSPA, the details of which warrant further analysis in the future.

In summary, the pH modulation technique is quite simple and sensitive. The assay just needs one simple labeling process, as opposed to Förster resonance energy transfer (FRET) techniques, which require labeling of two different fluorescent dyes at specific sites. Also this method utilizes a fluorometer, which is common in most labs, to demonstrate nM sensitivities. This sensitivity can be optimized if specific site labeling of fluorophores is utilized. This would help to reduce background fluorescence from dyes that are far away from the binding sites and are thus eliciting no response.

CHAPTER V

DESIGN AND ASSEMBLY OF INEXPENSIVE FLUORESCENCE DETECTOR

Introduction

A fluorescence microscope is an optical microscope that utilizes fluorescence and phosphorescence emission in addition to, or instead of, absorption and reflection of white light in studying properties of biological or non-biological substances.[154] The generation of a fluorescence image could be through several kinds of set up, such as epi-fluorescence microscope, which is the simplest one, and confocal microscope, which utilizes optical sectioning in order to obtain a fluorescent image with better resolution. With a wide variety of commercial available fluorescence dye molecules and fluorescent proteins, as well as different labeling methods, fluorescence sensing method provides target-specific, high-contrast images possible for quantitative, multiplexed and automated data analysis.[155-159] As a result, the measurement of förster resonance energy transfer (FRET), fluorescence recovery after photobleaching (FRAP), single molecule fluorescence study et al. has been made feasible.

In our laboratory, the epi-fluorescence microscope is the major device utilized in monitoring the fluorescence intensity in the label free pH modulation based sensing assays. This equipment is also very common in life science related laboratories. The design of such a microscope is schematically illustrated in Figure 5.1. The excitation light is generated by selecting out the right wavelength light with a band pass filter from the white light emitted by a mercury lamp. This emission light is later reflected by a

dichroic mirror and focused by an objective lens to the sample stage. The emitted fluorescence light are collected by the objective lens, filtered by the long pass emission filter, and finally directed to the detector that is usually a deep cooled CCD chip. The sensitivity of such an epi-fluorescence microscope mostly depends on the numerical aperture of the objective lens, which defines the angle that the system can accept the light from, and the cooling temperature for the CCD chip, which eliminates the thermo noises.

Although there are great advantages for these fluorescence microscopes, they do have inherent disadvantages of high cost, large size, and limited field of view.[160] An alternative fluorescence imaging system that could resolve these drawbacks can greatly compensate the deficiency of fluorescence microscopes in certain assays.

Previously, we developed fluorescence pH modulation bio-sensing platform, which has been demonstrated to be quite powerful in detecting protein-target interactions and drug-membrane interactions. During the development of this sensing platform, we used fluorescence microscopes to monitor the fluorescence intensity all the time. However, an expensive and bulky fluorescence microscope leads to high assay cost and limits the utilization of this method within a laboratory. With a brief research over the web, it's found that key components in a fluorescence microscope could be substituted by the commercialized cameras, schott glass filters, and the laser pointers, which have been well developed with pretty low cost on market. Thus, we were engaging in designing and building up a family affordable fluorescence detector costing under

several hundred dollars. The capacity of this device in our pH modulation assay was demonstrated by monitoring tetracaine-POPC SLB interaction.

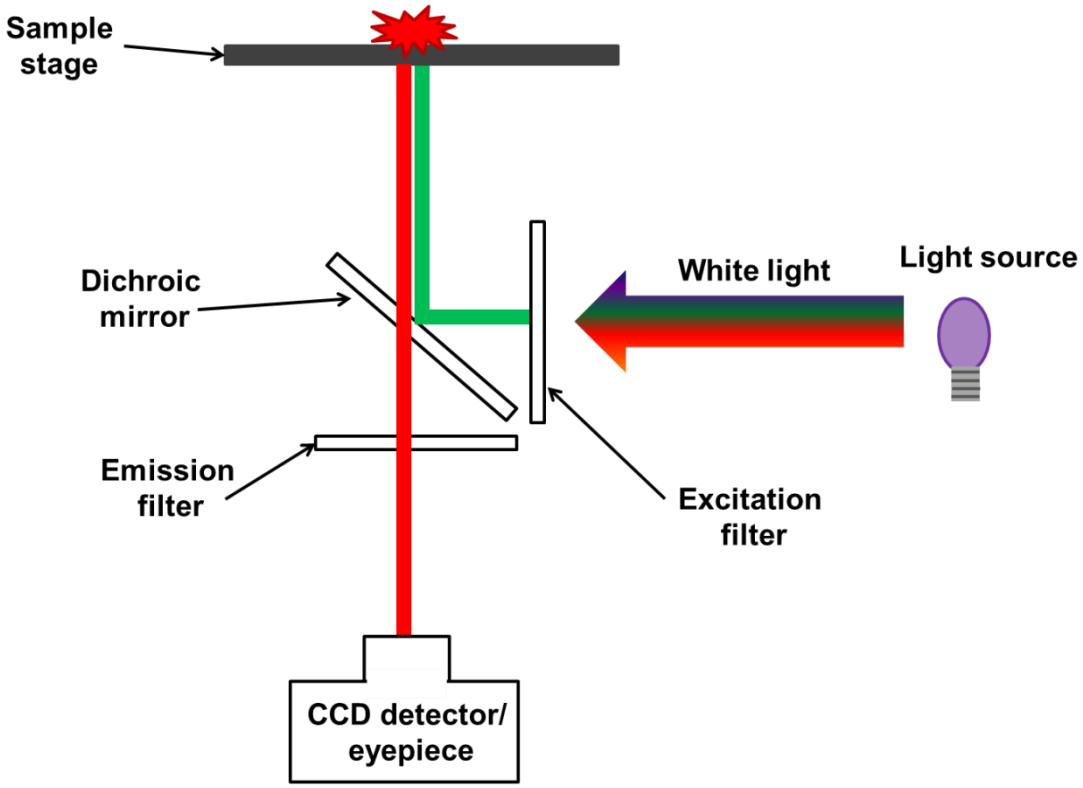

Figure 5.1. Schematic Diagram of Epi-fluorescence Microscopy. The excitation light is generated by a mercury lamp. A filter set is utilized to filter out the excitation and emission light. And a CCD detector is used for the detection of fluorescence emission intensity.

Inexpensive Fluorescence Detector Fabrication Results and Discussion

Device Fabrication. Considering that *ortho*-rhodamine B dye was utilized in our pH modulation bio-sensing platform,[25, 27] a 532 nm laser pointer was selected as the excitation light source. Schott OG-570 coated glass filter that claimed to have its optical density value higher than 3 below the wavelength of 550 nm was utilized as the filter for the emission light. And a Cannon SX-120 powershot camera with manual operation mode was used as the detector. The fabrication has been introduced in Chapter II and shown in Figure 2.5.

Laser Illumination Characterization. Other than avoiding the direct reflection of laser light into the camera lens that may cause huge background noise, mounting the laser pointer at an angle to the sample stage could change a the shape of the laser from a small round point to a elongated ellipse. This enables the illumination over a short range that may cover all the channels on a single microfluidic device. However, this elongated ellipse laser spot needs to be uniform enough for direct comparison among the intensity of those microfluidic channels. To characterize this illumination, approximately 3 μm thick MICROPOSIT S1813 photoresist was spin-coated onto a large microscope glass slide. The glass slide was then mounted onto the sample stage on the fluorescence microscope and monitored by the mounted deep cooled CCD. The illumination was switched between the mounted Prior Scientific Lumen 200 Fluorescence Illumination System and the tilted laser pointer. As shown in Figure 5.2, the line scan over the illuminated area indicates the tilted laser pointer could give a relatively even

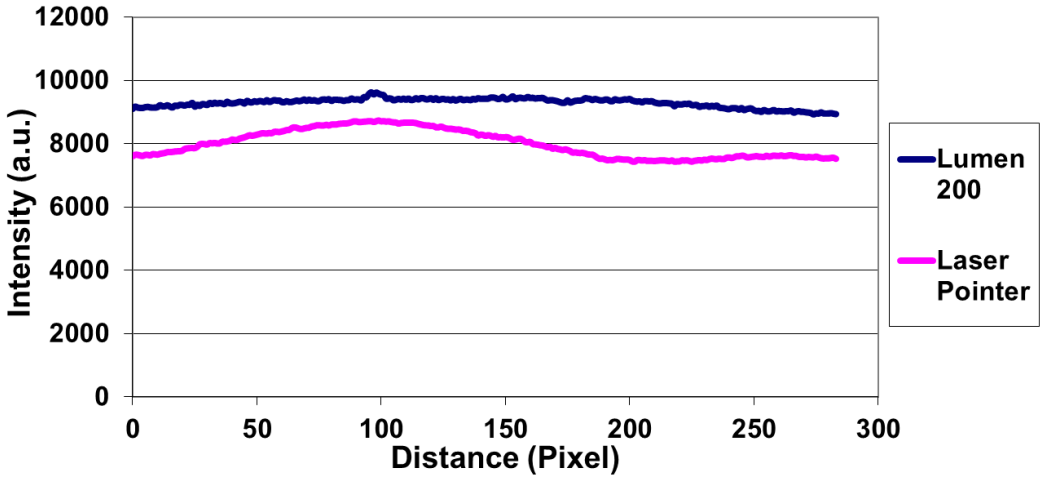

Figure 5.2. Intensity Scan for Excitation Illumination. The figure shows the intensity line scans over the illuminated area by Lumen 200 Fluorescence Illumination System (Blue) and tilted laser pointer (Pink) respectively.

illumination over the whole illuminated area, which has no obvious vignetting phenomenon and is comparable to the Lumen 200 Fluorescence Illumination System. Also, the existing illumination inhomogeneity could be adjusted simply by background subtraction.

System Characterization. Noise level, which determines the detection limit in sensing assays, is an important property of a system. In our case, this noise level majorly depends on the performance of the detector, which relies on the cooling temperature. Through deep cooling method, it could help reduce dark current and improve the CCD sensitivity. However, on the simplest design, it is not realistic to adopt a deep cooling system to the Canon camera in our inexpensive fluorescence detector, which may impede the portability of designed device. As a result, it requires testing the signal to noise level of the inexpensive fluorescence detector in order to estimate its performance compared to a fluorescence microscope. On the other hand, our pH modulation sensing platform monitors the fluorescence intensity of the sample, which correlates with the concentration/amount of the analyst. This correlation is believed to be linear if the intensity measured from an image is proportional to the actual fluorescence intensity emitted from the sample. Thus, to switch to our inexpensive fluorescence detector for pH modulation assays, it is necessary to prove that this kind of linear response still exists.

To test the signal to noise ratio and the linear response of fluorescence intensity of our inexpensive fluorescence detector and compare the results with the fluorescence microscope, a microfluidic device with different concentrations of POPC lipid vesicles with 0.5 mol% *para*-rhodamine B-POPE lipid in 50 mM pH 7.0 PBS buffer in each

channel is monitored by both system. As shown in 5.3(a) and 5.3(b), our inexpensive fluorescence detector could obtain a decent fluorescence picture of the sample in the microfluidic device, which is similar to the picture obtained from the fluorescence microscope system. The line scan over these two pictures (Figure 5.3(c) and 5.3(d)) gives an estimation of signal to noise ration for these two systems respectively. For the fluorescence microscope, the signal to noise ratio is 175, while for the inexpensive fluorescence detector the value is 42. Although the signal to noise ratio of inexpensive fluorescence detector is over four times less than the fluorescence microscope, this signal to noise ratio could still be enough for the general measurement in our pH modulation assays. By taking and overlapping multiple pictures for the same device, it is feasible to greatly decrease this noise level and increase the sensitivity. With several repeats and averaging the intensity data, the linear response of the inexpensive fluorescence detector is demonstrated (Figure 5.3(f)), which is comparable to the fluorescence microscope (Figure 5.3(e)). The large error bar in Figure 5.3(f) is mostly due to the relatively higher noise level of the system.

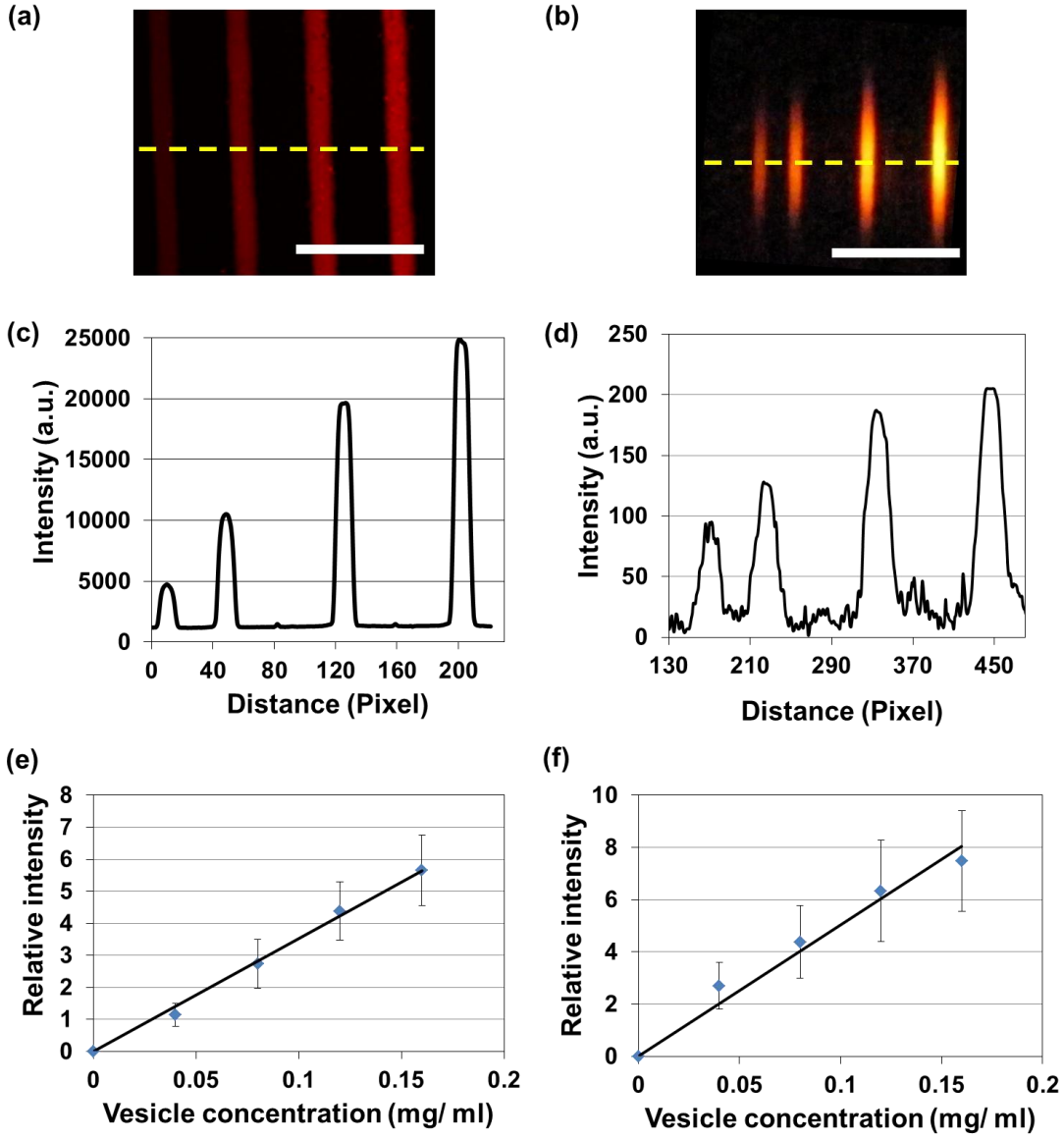

Figure 5.3. System Characterization. The measurement of the linear response of fluorescence intensity from fluorescence microscope system and our inexpensive fluorescence detector is shown. (a) is the picture taken from the microscope system, and (b) is the picture taken from our inexpensive detector. The yellow dot line indicates the location of the intensity line scan. The white solid line is the scale bar, which is 0.5 mm. (c) and (d) shows the intensity line scan of (a) and (b) respectively. (e) and (f) summarize the averaged data and shows the linear response of microscope system and our inexpensive fluorescence detector with increasing concentration of dye labeled vesicles in the injected buffer solution.

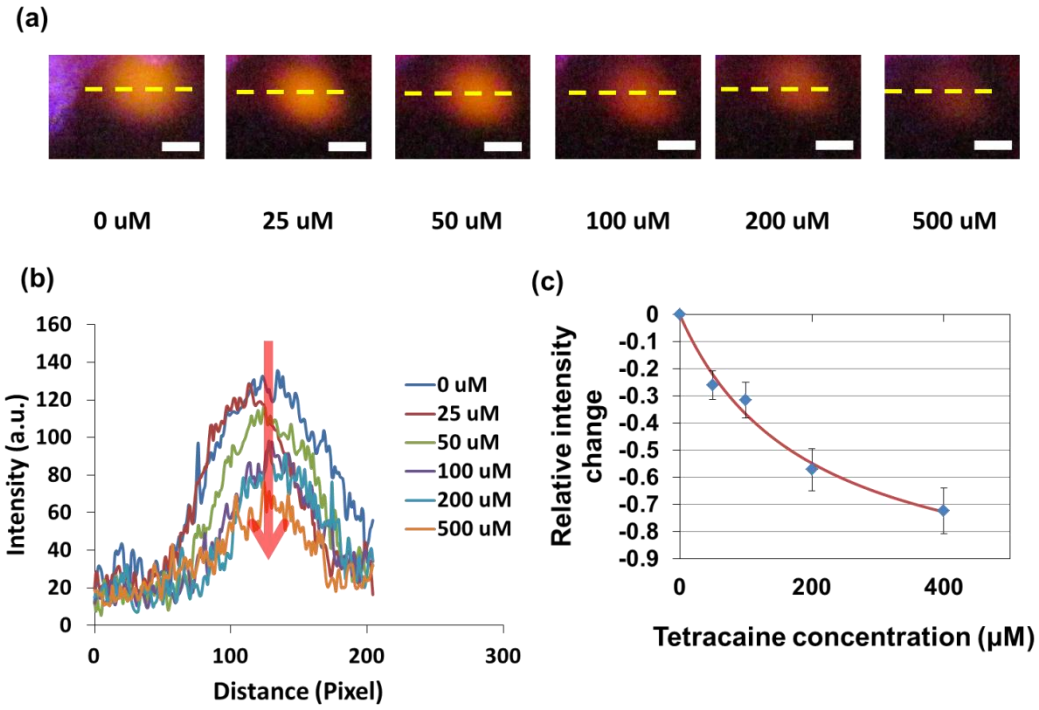

Figure 5.4. Application of Inexpensive Fluorescence Detector. (a) The fluorescence pictures obtained by our inexpensive fluorescence detector on the POPC bilayer in the flow cell under different bulk tetracaine concentrations (0-500 μM). The yellow dot line indicates the location of the intensity line scan. The white solid line is the scale bar, which is 1 mm. (b) Line scan profiles for the pictures in (a). (c) Plot of relative fluorescence intensity change vs. bulk tetracaine concentration. The red solid line is the best Langmuir isotherm fit to the data points.

Flow Cell Measurement. Based on these characterizations, this newly designed inexpensive fluorescence detector was utilized to monitor the fluorescence intensity in our pH modulation assay. Initially, the experiment was carried out with a flow cell, which is similar to the one used in chapter III. And SLBs containing 99.5 mol% POPC and 0.5 mol% oRB-PE were utilized. This work was performed in 50 mM sodium phosphate buffer at pH 7.1 ± 0.1.[87] The buffer was flowed over the patterned bilayers until fluorescence stabilization was achieved. Next, tetracaine at different concentrations ranging from 0-500 μM was introduced into the buffer and continuously flowed through the flow cell until the fluorescence intensity from the lipid bilayer stabilized. Images were captured after 30 minutes' stabilization.

A series of images after equilibration with 0-500 μM tetracaine with phosphate buffer are shown in Figure 5.4(a). It is very obvious that the intensity of this orange dot, which is the fluorescence emission from the POPC SLB, decreased with increasing concentration of tetracaine molecule. The individual fluorescence line scans for 8 tetracaine concentrations, indicated as yellow dot lines in Figure 5.4(a), are shown in Figure 5.4(b). At the highest concentration of tetracaine employed, 500 μM, the fluorescence intensity decreased by more than a factor of three.

Using the data from Figure 5.4(b), the relative fluorescence intensity decrease could be plot as a function of drug molecule concentration (Figure 5.4(c)). The y-axis represents the relative fluorescence change ΔF, which is calculated as $(F-F_0)/F_0$, i.e. F/F_0-1. In this equation, F is the fluorescence intensity of the bilayer as a function of

tetracaine concentration in the bulk solution, whereas F_0 is the fluorescence intensity of the bilayer in pure buffer.

The data in Figure 5.4(c) can be fit to a Langmuir isotherm as shown by the red solid line. The apparent equilibrium dissociation constant is abstracted using equation 5.1:

$$\Delta F = -a\frac{[T]}{K_D+[T]} \tag{5.1}$$

where T is the bulk concentration of tetracaine and a is a constant corresponding to the maximum relative fluorescence intensity change. The fit yields a K_d of 266 ± 43 μM, which is consistent with the literature value for this binding event found by non-linear optical measurements.[34]

Discussion. In the current design and assembly method, all the parts are fixed in place on a laser table. This device could give a decent signal to noise ratio compared to a deep cooled CCD chip on a fluorescence microscope when the fluorescence emission intensity is strong enough as shown in Figure 5.3, in which dye labeled vesicle solutions were utilized. However, when the sample's fluorescence intensity is pretty weak, such as the fluorescence emitted from SLBs, the noise level increased dramatically, which limits the sensitivity a lot. Thus, in the future development of this kind of device, a proper cooling method may be designed without too much cost. And dark paper may be needed to absorb all the diffracted light.

On the other hand, it worth noting that there is no lock and key like fitting site on the sample stage for the device mounted such as the flow cell here. Thus, double side tape was utilized for the mounting purpose. Although this kind of tape works perfectly in

fixing the device in place, it is very difficult to remount the device at exactly the same place on the sample stage in different repeated experiments. This could lose the repeatability of the assay and cause a lot of effort in re-aligning the laser pointer and the camera. In order to solve this problem, it is planed to design and make a 3D plastic box that has all the pre-designed mounting sites for each component. Also, such a box could enable the adopting of a cooling system and some other light blocking and absorption pieces.

Finally, with the technology development in recent years, almost every cell phone has an integrated camera. These integrated cameras sometimes are even better than an individual camera on aspects like resolution and sensitivity. If a cell phone integrated camera could be utilized in our device, it will make the design even more portable and cost efficient as there will be no need in having an extra camera. However, in current design, a manual function for the camera is necessary, which most of the cell phone integrated cameras do not have. If the camera is in auto mode, slight setting change when taking the images will make it impossible to compare two pictures and extract useful data. For example, in the flow cell attempt, if the exposure time is different for those images in Figure 5.4(a), the intensity data from the line scan will no longer be valid for comparison. Also, the weak fluorescence light makes it very difficult for auto focusing. We believe by just including a simple program that enables manual controlling the camera could resolve the conflict easily. And this will be the future direction of the development.

Conclusions

As a conclusion, it has been successfully demonstrated that our newly designed and built inexpensive fluorescence detector could give a decent signal to noise ratio in fluorescence intensity measurement compared to the fluorescence microscope. Later on, this fluorescence detector was utilized in the pH modulation assays in which the interaction between tetracaine, an anesthetic drug molecule, and POPC SLB was studied. Although the signal to noise ratio is not as good as a fluorescence microscope in the sensing assays, by averaging the data, it is still able to obtain the correct thermodynamics data.

By comparison, our inexpensive fluorescence detector has several advantages. Firstly and most importantly, this inexpensive fluorescence detector is really cheap, which only costs couple of hundred dollars in total. This price is approximately 2-3 orders of magnitude less than that of an epi-fluorescence microscope. Such cheap price will enable the possession of this inexpensive fluorescence detector for each single family, which promotes the everyday application of those fluorescence based assays. Also, this price could be even lowered if the cell phone camera is utilized. Secondly, this newly designed fluorescence detector is portable. The microscope part of an epi-fluorescence microscope, which has many delicate parts, is quite heavy in tens of kilograms. As a result, the microscope could only be set on certain flat and sturdy surfaces, avoiding being moved too frequently. Also, the deep cooled CCD detector and the mercury lamp have never been considered to be portable as they are also relatively big in size. With our new design, the whole weight of the detector will be less than 5

kilograms. And the size of this detector could be smaller than 20 cm^3. Thirdly, this detector could be developed into an automated detector that does not need specially trained operators. With the help of a designed plastic box, each component could be fixed in place and tuned by mini-motors. It is believed that with the help of a simple computer program, the automated sensing could be realized.

CHAPTER VI

CONCLUSIONS

We have developed a new label free fluorescence based pH modulation sensing method that makes use of a pH sensitive fluorescent dye in sensing the local pH changes of a SLB upon the binding between a ligand and a receptor on the SLB surface. It is able to tune the sensing pH range by adjusting the buffer concentration as well as the buffer ionic strength. Based on the previous study, this sensing platform has been successfully applied in the field of monitoring drug-membrane interactions. Tetracaine, a well-studied anesthetic drug, has been selected as the model drug. By utilizing the pH modulation method, it is able to obtain the thermodynamics data of the interaction between tetracaine and POPC SLB. The composition of the bilayer could be modulated with the incorporation of nature cell membrane components, such as cholesterol, POPE lipid, and some negatively charged lipids. This enables the study and analysis on how the nature of different membrane components influences the interaction between the drug molecule and the SLB. In the future, it is anticipated that this kind of technique could be utilized in new drug development, in which this could be used in screening out the target drug molecule that has anticipated proper interaction with the cell membrane. Also, this method could be used for the study of drug-membrane protein interactions, which is under development in our laboratory.

Based on the prototype of this pH modulation sensing platform, it is very useful if this assay platform could be extended for homogeneous studies, such as protein-target association measurement. By comparison, a protein backbone could work as the lipid

bilayer that accommodates the target molecule recognition site and the pH sensitive fluorescence dye molecules. Through the demonstration on sensing rSPA-IgG, TbPA-ThMP, and Calmodulin-Ca^{2+} interactions, pH modulation based sensing method has been successfully extended to a homogeneous sensing platform. With the success of this design, it is hoped that this kind of sensor could be applied in detection small molecules and ions selectively, such as detecting the pollutant of Hg^{2+} in the river around Texas.

Finally, the high cost and cumbersome of a fluorescence microscope could inevitably prevent the wide application of our newly developed sensing platform. To address this issue, a design for an inexpensive microscope substitute was carried out. A common camera, a schott glass filter, and a 532 nm laser pointer could be enough for the substitution of the key components on a fluorescence microscope. And all of these only cost several hundred dollars. Based on these components, an inexpensive fluorescence detector was successfully built, characterized, and tested in the study of tetracaine-POPC SLB interaction. Still, this kind of inexpensive fluorescence detector is under further development. Firstly, we designed a plastic box to fix each component in place. Several mini motors could be utilized to tune the direction of the laser pointer, the sample stage, and the camera. The cell phone integrated camera could be used to substitute the Canon camera here to further bring down the cost of the device and increase the portability of it.

REFERENCES

1. Albanese, J.; Dainiak, N., *Exp. Hematol.* **2003**, *31*, 455-464.

2. Ross, G. D.; Vetvicka, V., *Clin. Exp. Immunol.* **1993**, *92*, 181-184.

3. Mammen, M.; Choi, S. K.; Whitesides, G. M., *Angew. Chem. Int. Edit.* **1998**, *37*, 2755-2794.

4. Bechinger, B.; Salnikov, E. S., *Chem. Phys. Lipids* **2012**, *165*, 282-301.

5. Stromstedt, A. A.; Ringstad, L.; Schmidtchen, A.; Malmsten, M., *Curr. Opin. Colloid Interface Sci.* **2010**, *15*, 467-478.

6. Jung, H.; Robison, A. D.; Cremer, P. S., *J. Struct. Biol.* **2009**, *168*, 90-94.

7. Yang, T. L.; Baryshnikova, O. K.; Mao, H. B.; Holden, M. A.; Cremer, P. S., *J. Am. Chem. Soc.* **2003**, *125*, 4779-4784.

8. Shi, J. J.; Yang, T. L.; Kataoka, S.; Zhang, Y. J.; Diaz, A. J.; Cremer, P. S., *J. Am. Chem. Soc.* **2007**, *129*, 5954-5961.

9. Haab, B. B., *Proteomics* **2003**, *3*, 2116-2122.

10. Yu, X. B.; Xu, D. K.; Cheng, Q., *Proteomics* **2006**, *6*, 5493-5503.

11. Cooper, M. A., *J. Mol. Recogn.* **2004**, *17*, 286-315.

12. Kuziemko, G. M.; Stroh, M.; Stevens, R. C., *Biochemistry-Us* **1996**, *35*, 6375-6384.

13. Ellson, C. D.; Gobert-Gosse, S.; Anderson, K. E.; Davidson, K.; Erdjument-Bromage, H.; Tempst, P.; Thuring, J. W.; Cooper, M. A.; Lim, Z. Y.; Holmes, A. B.; Gaffney, P. R. J.; Coadwell, J.; Chilvers, E. R.; Hawkins, P. T.; Stephens, L. R., *Nat. Cell. Biol.* **2001**, *3*, 679-682.

14. Stahelin, R. V.; Burian, A.; Bruzik, K. S.; Murray, D.; Cho, W. W., *J. Biol. Chem.* **2003**, *278*, 14469-14479.

15. Cooper, M. A.; Williams, D. H., *Chem. Biol.* **1999**, *6*, 891-899.

16. Ahijado-Guzman, R.; Gomez-Puertas, P.; Alvarez-Puebla, R. A.; Rivas, G.; Liz-Marzan, L. M., *Acs Nano* **2012**, *6*, 7514-7520.

17. Banerjee, A.; Perez-Castillejos, R.; Hahn, D.; Smirnov, A. I.; Grebel, H., *Chem. Phys. Lett.* **2010**, *489*, 121-126.

18. Patel, A. R.; Kanazawa, K. K.; Frank, C. W., *Anal. Chem.* **2009**, *81*, 6021-6029.

19. Buzhynskyy, N.; Golczak, M.; Lai-Kee-Him, J.; Lambert, O.; Tessier, B.; Gounou, C.; Berat, R.; Simon, A.; Granier, T.; Chevalier, J. M.; Mazeres, S.; Bandorowicz-Pikula, J.; Pikula, S.; Brisson, A. R., *J. Struct. Biol.* **2009**, *168*, 107-116.

20. Braun, T.; Ghatkesar, M. K.; Backmann, N.; Grange, W.; Boulanger, P.; Letellier, L.; Lang, H. P.; Bietsch, A.; Gerber, C.; Hegner, M., *Nat. Nanotechnol.* **2009**, *4*, 179-185.

21. Zhang, Y. F.; Venkatachalan, S. P.; Xu, H.; Xu, X. H.; Joshi, P.; Ji, H. F.; Schulte, M., *Biosens. Bioelectron.* **2004**, *19*, 1473-1478.

22. Heerklotz, H., *J. Phys.: Condens. Matter* **2004**, *16*, R441-R467.

23. Conboy, J. C.; Kriech, M. A., *Anal. Chim. Acta* **2003**, *496*, 143-153.

24. Wei, F.; Ye, S. J.; Li, H. C.; Luo, Y., *J. Phys. Chem. C* **2013**, *117*, 11095-11103.

25. Jung, H.; Robison, A. D.; Cremer, P. S., *J. Am. Chem. Soc.* **2009**, *131*, 1006-1014.

26. Cremer, P. S.; Boxer, S. G., *J. Phys. Chem. B* **1999**, *103*, 2554-2559.

27. Robison, A. D. H., D.; Jung, H.; Cremer, P. S., *Biointerphases* **2013**, *8*, 1-9.

28. McNeely, P. M.; Naranjo, A. N.; Robinson, A. S., *Biotechnol. J.* **2012**, *7*, 1451-1461.

29. Rask-Andersen, M.; Almen, M. S.; Schioth, H. B., *Nat. Rev. Drug. Discov.* **2011**, *10*, 579-590.

30. Austin, R. P.; Barton, P.; Davis, A. M.; Fessey, R. E.; Wenlock, M. C., *Pharm. Res.* **2005**, *22*, 1649-1657.

31. Fisar, Z.; Fuksova, K.; Velenovska, M., *Gen. Physiol. Biophys.* **2004**, *23*, 77-99.

32. Howell, B. A.; Chauhan, A., *Langmuir* **2009**, *25*, 12056-12065.

33. Pajeva, I. K.; Wiese, M.; Cordes, H. P.; Seydel, J. K., *J. Cancer Res. Clin. Oncol.* **1996**, *122*, 27-40.

34. Nguyen, T. T.; Conboy, J. C., *Anal. Chem.* **2011**, *83*, 5979-5988.

35. Bornhop, D. J.; Latham, J. C.; Kussrow, A.; Markov, D. A.; Jones, R. D.; Sorensen, H. S., *Science* **2007**, *317*, 1732-1736.

36. Li, Y. C.; Chang, Y. F.; Su, L. C.; Chou, C., *Anal. Chem.* **2008**, *80*, 5590-5595.

37. Hoffman, T. L.; Canziani, G.; Jia, L.; Rucker, J.; Doms, R. W., *Proc. Natl. Acad. Sci. U. S. A.* **2000**, *97*, 11215-11220.

38. Raorane, D. A.; Lim, M. D.; Chen, F. F.; Craik, C. S.; Majumdar, A., *Nano Lett.* **2008**, *8*, 2968-2974.

39. Zhang, G. J.; Huang, M. J.; Luo, Z. H.; Tay, G. K.; Lim, E. J.; Liu, E. T.; Thomsen, J. S., *Biosens. Bioelectron.* **2010**, *26*, 365-370.

40. Kerby, M. B.; Legge, R. S.; Tripathi, A., *Anal. Chem.* **2006**, *78*, 8273-8280.

41. Wang, K. I. K.; Salcic, Z.; Yeh, J.; Akagi, J.; Zhu, F.; Hall, C. J.; Crosier, K. E.; Crosier, P. S.; Wlodkowic, D., *Biosens. Bioelectron.* **2013**, *48*, 188-196.

42. Guo, J.; Zhang, J. J.; Thomas, S.; Sonkusale, S., *IEEE Sens. J.* **2012**, *12*, 2506-2507.

43. Murari, K.; Etienne-Cummings, R.; Thakor, N. V.; Cauwenberghs, G., *IEEE T. Biomed. Circ. S.* **2011**, *5*, 449-458.

44. Dewa, T.; Sugiura, R.; Suemori, Y.; Sugimoto, M.; Takeuchi, T.; Hiro, A.; Iida, K.; Gardiner, A. T.; Cogdell, R. J.; Nango, M., *Langmuir* **2006**, *22*, 5412-5418.

45. Tero, R.; Ujihara, T.; Urisut, T., *Langmuir* **2008**, *24*, 11567-11576.

46. Brian, A. A.; McConnell, H. M., *Proc. Natl. Acad. Sci. U. S. A.* **1984**, *81*, 6159-6163.

47. Mcconnell, H. M.; Watts, T. H.; Weis, R. M.; Brian, A. A., *Biochim. Biophys. Acta.* **1986**, *864*, 95-106.

48. Laggner, P.; Gotto, A. M.; Morrisett, J. D., *Biochemistry-Us* **1979**, *18*, 164-171.

49. Sadler, D. M.; Reisshusson, F.; Rivas, E., *Chem. Phys. Lipids* **1990**, *52*, 41-48.

50. Knoll, W.; Haas, J.; Stuhrmann, H. B.; Fuldner, H. H.; Vogel, H.; Sackmann, E., *J. Appl. Crystallogr.* **1981**, *14*, 191-202.

51. Yang, T. L.; Jung, S. Y.; Mao, H. B.; Cremer, P. S., *Anal. Chem.* **2001**, *73*, 165-169.

52. Holden, M. A.; Cremer, P. S., *J. Am. Chem. Soc.* **2003**, *125*, 8074-8075.

53. Castellana, E. T.; Cremer, P. S., *Biointerphases* **2007**, *2*, 57-63.

54. Kang, L. F.; Chung, B. G.; Langer, R.; Khademhosseini, A., *Drug Discov. Today* **2008**, *13*, 1-13.

55. Lee, J.; Soper, S. A.; Murray, K. K., *Anal. Chim. Acta* **2009**, *649*, 180-190.

56. Ben-Yakar, A.; Chronis, N.; Lu, H., *Curr. Opin. Neurobiol.* **2009**, *19*, 561-567.

57. Duffy, D. C.; McDonald, J. C.; Schueller, O. J. A.; Whitesides, G. M., *Anal. Chem.* **1998**, *70*, 4974-4984.

58. Delamarche, E.; Schmid, H.; Michel, B.; Biebuyck, H., *Adv. Mater.* **1997**, *9*, 741-746.

59. Paguirigan, A. L.; Beebe, D. J., *Integr. Biol.* **2009**, *1*, 182-195.

60. Jung, H. S.; Yang, T.; Lasagna, M. D.; Shi, J. J.; Reinhart, G. D.; Cremer, P. S., *Biophys. J.* **2008**, *94*, 3094-3103.

61. Liu, C. M.; Monson, C. F.; Yang, T. L.; Pace, H.; Cremer, P. S., *Anal. Chem.* **2011**, *83*, 7876-7880.

62. Castellana, E. T.; Cremer, P. S., *Surf. Sci. Rep.* **2006**, *61*, 429-444.

63. Custodio, J. B. A.; Almeida, L. M.; Madeira, V. M. C., *Biochem. Biophys. Res. Commun.* **1991**, *176*, 1079-1085.

64. Auger, M.; Jarrell, H. C.; Smith, I. C. P., *Biochemistry-Us* **1988**, *27*, 4660-4667.

65. Peng, X. D.; Jonas, A.; Jonas, J., *Chem. Phys. Lipids* **1995**, *75*, 59-69.

66. Castro, V.; Stevensson, B.; Dvinskikh, S. V.; Hogberg, C. J.; Lyubartsev, A. P.; Zimmermann, H.; Sandstrom, D.; Maliniak, A., *BBA-Biomembranes* **2008**, *1778*, 2604-2611.

67. De Paula, E.; Schreier, S., *BBA-Biomembranes* **1995**, *1240*, 25-33.

68. Paiva, J. G.; Paradiso, P.; Serro, A. P.; Fernandes, A.; Saramago, B., *Colloids and Surfaces B-Biointerfaces* **2012**, *95*, 65-74.

69. Moreno, M. M.; Garidel, P.; Suwalsky, M.; Howe, J.; Brandenburg, K., *BBA-Biomembranes* **2009**, *1788*, 1296-1303.

70. Shibata, A.; Ikawa, K.; Terada, H., *Biophys. J.* **1995**, *69*, 470-477.

71. Auger, M.; Smith, I. C. P.; Mantsch, H. H.; Wong, P. T. T., *Biochemistry-Us* **1990**, *29*, 2008-2015.

72. Fox, C. B.; Harris, J. M., *J. Raman Spectrosc.* **2010**, *41*, 498-507.

73. Fox, C. B.; Horton, R. A.; Harris, J. M., *Anal. Chem.* **2006**, *78*, 4918-4924.

74. Nguyen, T. T.; Rembert, K.; Conboy, J. C., *J. Am. Chem. Soc.* **2009**, *131*, 1401-1403.

75. Tokarska-Schlattner, M.; Epand, R. F.; Meiler, F.; Zandomeneghi, G.; Neumann, D.; Widmer, H. R.; Meier, B. H.; Epand, R. M.; Saks, V.; Wallimann, T.; Schlattner, U., *Plos One* **2012**, *7*, 1-11.

76. Lucio, M.; Bringezu, F.; Reis, S.; Lima, J. L. F. C.; Brezesinski, G., *Langmuir* **2008**, *24*, 4132-4139.

77. Zhang, J. Z.; Hadlock, T.; Gent, A.; Strichartz, G. R., *Biophys. J.* **2007**, *92*, 3988-4001.

78. Sackmann, E., *Science* **1996**, *271*, 43-48.

79. Cremer, P. S.; Groves, J. T.; Kung, L. A.; Boxer, S. G., *Langmuir* **1999**, *15*, 3893-3896.

80. Liu, Y.; Liao, P.; Cheng, Q.; Hooley, R. J., *J. Am. Chem. Soc.* **2010**, *132*, 10383-10390.

81. Kissler, S.; Pierrat, S.; Zimmermann, T.; Vogt, H.; Trieu, H. K.; Koper, I., *Biomed. Tech./Biomed. Eng.* **2012**, *57*, 1010-1013.

82. Benkoski, J. J.; Jesorka, A.; Kasemo, B.; Hook, F., *Macromolecules* **2005**, *38*, 3852-3860.

83. Joubert, J. R.; Smith, K. A.; Johnson, E.; Keogh, J. P.; Wysocki, V. H.; Gale, B. K.; Conboy, J. C.; Saavedra, S. S., *ACS Appl. Mater. Interfaces* **2009**, *1*, 1310-1315.

84. Forstner, M. B.; Yee, C. K.; Parikh, A. N.; Groves, J. T., *J. Am. Chem. Soc.* **2006**, *128*, 15221-15227.

85. Szmodis, A. W. B., C. D.; Longo, M. L.; Orme, C. A.; Parikh, A. N., *Biointerphases* **2010**, *5*, 120-130.

86. Huang, D.; Robison, A. D.; Liu, Y. Q.; Cremer, P. S., *Biosens. Bioelectron.* **2012**, *38*, 74-78.

87. Robison, A. D., Huang, D.; Jung, H.; Cremer, P. S., *Biointerphases* **2013**, *8*, 1-9.

88. Fodor, A. A.; Gordon, S. E.; Zagotta, W. N., *J. Gen. Physiol.* **1997**, *109*, 3-14.

89. Roth, S. H., *Annu. Rev. Pharmacol. Toxicol.* **1979**, *19*, 159-178.

90. Lee, A. G., *Nature* **1976**, *262*, 545-548.

91. Weizenmann, N.; Huster, D.; Scheidt, H. A., *BBA-Biomembranes* **2012**, *1818*, 3010-3018.

92. Hutterer, R.; Kramer, K.; Schneider, F. W.; Hof, M., *Chem. Phys. Lipids* **1997**, *90*, 11-23.

93. Kuroda, Y.; Fujiwara, Y., *Biochim. Biophys. Acta.* **1987**, *903*, 395-410.

94. Cansell, M.; Gouygou, J. P.; Jozefonvicz, J.; Letourneur, D., *Lipids* **1997**, *32*, 39-44.

95. Corvera, S.; DiBonaventura, C.; Shpetner, H. S., *J. Biol. Chem.* **2000**, *275*, 31414-31421.

96. Ikonen, E., *Nat. Rev. Mol. Cell. Bio.* **2008**, *9*, 125-138.

97. Kim, K.; Kim, C.; Byun, Y., *Langmuir* **2001**, *17*, 5066-5070.

98. Vance, J. E., *J. Lipid Res.* **2008**, *49*, 1377-1387.

99. Tsui, F. C.; Ojcius, D. M.; Hubbell, W. L., *Biophys. J.* **1986**, *49*, 459-468.

100. Hamai, C.; Yang, T. L.; Kataoka, S.; Cremer, P. S.; Musser, S. M., *Biophys. J.* **2006**, *90*, 1241-1248.

101. Herrera, F. E.; Bouchet, A.; Lairion, F.; Disalvo, E. A.; Pantano, S., *J. Phys. Chem. B* **2012**, *116*, 4476-4483.

102. Nussio, M. R.; Voelcker, N. H.; Sykes, M. J.; McInnes, S. J. P.; Gibson, C. T.; Lowe, R. D.; Miners, J. O.; Shapter, J. G., *Biointerphases* **2008**, *3*, 96-104.

103. Pink, D. A.; McNeil, S.; Quinn, B.; Zuckermann, M. J., *BBA-Biomembranes* **1998**, *1368*, 289-305.

104. Sen, A.; Yang, P. W.; Mantsch, H. H.; Hui, S. W., *Chem. Phys. Lipids* **1988**, *47*, 109-116.

105. Ho, C.; Slater, S. J.; Stubbs, C. D., *Biochemistry-Us* **1995**, *34*, 6188-6195.

106. Kelusky, E. C.; Smith, I. C., *Biochemistry-Us* **1983**, *22*, 6011-6017.

107. Shintou, K.; Nakano, M.; Kamo, T.; Kuroda, Y.; Handa, T., *Biophys. J.* **2007**, *93*, 3900-3906.

108. Hornby, A. P.; Cullis, P. R., *Biochim. Biophys. Acta.* **1981**, *647*, 285-292.

109. Borkenhagen, L.; Kennedy, E. P.; Fielding, L., *J. Biol. Chem.* **1961**, *236*, PC28-PC30.

110. Yeung, T.; Gilbert, G. E.; Shi, J.; Silvius, J.; Kapus, A.; Grinstein, S., *Science* **2008**, *319*, 210-213.

111. Grenache, D. G.; Gronowski, A. M., *Clin. Biochem.* **2006**, *39*, 1-10.

112. Seddon, A. M.; Lorch, M.; Ces, O.; Templer, R. H.; Macrae, F.; Booth, P. J., *J. Mol. Biol.* **2008**, *380*, 548-556.

113. Ohmi, Y.; Tajima, O.; Ohkawa, Y.; Yamauchi, Y.; Sugiura, Y.; Furukawa, K.; Furukawa, K., *J. Neurochem.* **2011**, *116*, 926-935.

114. Yu, R. K.; Tsai, Y. T.; Ariga, T., *Neurochem. Res.* **2012**, *37*, 1230-1244.

115. Monson, C. F.; Cong, X.; Robison, A. D.; Pace, H. P.; Liu, C.; Poyton, M. F.; Cremer, P. S., *J. Am. Chem. Soc.* **2012**, *134*, 7773-7779.

116. Nakagaki, M.; Katoh, I.; Handa, T., *Biochemistry-Us* **1981**, *20*, 2208-2212.

117. Smith, K. A.; Gale, B. K.; Conboy, J. C., *Anal. Chem.* **2008**, *80*, 7980-7987.

118. Rainsford, K. D., *Int. J. Clin. Pract.* **2013**, *67*, 9-20.

119. Jacobs, E. J.; Newton, C. C.; Gapstur, S. M.; Thun, M. J., *J. Natl. Cancer. I.* **2012**, *104*, 1208-1217.

120. Tahrani, A. A.; Piya, M. K.; Barnett, A. H., *Adv. Ther.* **2009**, *26*, 736-736.

121. Velazquez-Campoy, A.; Freire, E., *Biophys. Chem.* **2005**, *115*, 115-124.

122. Leavitt, S.; Freire, E., *Curr. Opin. Struct. Biol.* **2001**, *11*, 560-566.

123. Wiseman, T.; Williston, S.; Brandts, J. F.; Lin, L. N., *Anal. Biochem.* **1989**, *179*, 131-137.

124. Li, Y. C.; Chang, Y. F.; Su, L. C.; Chou, C., *Anal. Chem.* **2008**, *80*, 5590-5595.

125. Hoffman, T. L.; Canziani, G.; Jia, L.; Rucker, J.; Doms, R. W., *Proc. Natl. Acad. Sci. U. S. A.* **2000**, *97*, 11215-11220.

126. Raorane, D. A.; Lim, M. D.; Chen, F. F.; Craik, C. S.; Majumdar, A., *Nano Lett.* **2008**, *8*, 2968-2974.

127. Zhang, G. J.; Huang, M. J.; Luo, Z. H. H.; Tay, G. K. I.; Lim, E. J. A.; Liu, E. T.; Thomsen, J. S., *Biosens. Bioelectron.* **2010**, *26*, 365-370.

128. Kerby, M. B.; Legge, R. S.; Tripathi, A., *Anal. Chem.* **2006**, *78*, 8273-8280.

129. Lu, H. P.; Xun, L. Y.; Xie, X. S., *Science* **1998**, *282*, 1877-1882.

130. Xu, W. L.; Kong, J. S.; Yeh, Y. T. E.; Chen, P., *Nat. Mater.* **2008**, *7*, 992-996.

131. Kenaan, C.; Zhang, H. M.; Hollenberg, P. F., *Nat. Protoc.* **2010**, *5*, 1652-1658.

132. Boger, D. L.; Fink, B. E.; Brunette, S. R.; Tse, W. C.; Hedrick, M. P., *J. Am. Chem. Soc.* **2001**, *123*, 5878-5891.

133. Mahendrarajah, K.; Dalby, P. A.; Wilkinson, B.; Jackson, S. E.; Main, E. R. G., *Anal. Biochem.* **2011**, *411*, 155-157.

134. Nelson, N.; Sander, D.; Dandinf, M.; Sarje, A.; Prakash, S.; Ji, H. H.; Abshire, P., *IEEE Int. Symp. Circ. S.* **2008**, 1080-1083.

135. Vaasa, A.; Lust, M.; Terrin, A.; Uri, A.; Zaccolo, M., *Biochem. Biophys. Res. Commun.* **2010**, *397*, 750-755.

136. Mank, M.; Reiff, D. F.; Heim, N.; Friedrich, M. W.; Borst, A.; Griesbeck, O., *Biophys. J.* **2006**, *90*, 1790-1796.

137. Sapsford, K. E.; Berti, L.; Medintz, I. L., *Angew. Chem. Int. Edit.* **2006**, *45*, 4562-4588.

138. Mere, L.; Bennett, T.; Coassin, P.; England, P.; Hamman, B.; Rink, T.; Zimmerman, S.; Negulescu, P., *Drug Discov. Today* **1999**, *4*, 363-369.

139. Mordon, S.; Maunoury, V.; Devoisselle, J. M.; Abbas, Y.; Coustaud, D., *J. Photochem. Photobiol. B* **1992**, *13*, 307-314.

140. Langone, J. J., *Adv. Immunol.* **1982**, *32*, 157-252.

141. Saha, K.; Bender, F.; Gizeli, E., *Anal. Chem.* **2003**, *75*, 835-842.

142. Ogi, H.; Motohisa, K.; Hatanaka, K.; Ohmori, T.; Hirao, M.; Nishiyama, M., *Biosens. Bioelectron.* **2007**, *22*, 3238-3242.

143. Horisberger, M.; Clerc, M. F., *Eur. J. Cell Biol.* **1987**, *45*, 62-71.

144. Tracy, R. P.; Currie, R. M.; Kyle, R. A.; Young, D. S., *Clin. Chem.* **1982**, *28*, 900-907.

145. Hollenbach, A. D.; Dickson, K. A.; Washabaugh, M. W., *Protein. Expr. Purif.* **2002**, *25*, 508-518.

146. Soriano, E. V.; Rajashankar, K. R.; Hanes, J. W.; Bale, S.; Begley, T. P.; Ealick, S. E., *Biochemistry-Us* **2008**, *47*, 1346-1357.

147. Klee, C. B.; Crouch, T. H.; Richman, P. G., *Annu. Rev. Biochem.* **1980**, *49*, 489-515.

148. Teo, T. S.; Wang, J. H., *J. Biol. Chem.* **1973**, *248*, 5950-5955.

149. Liu, Y. P.; Lin, Y. M.; Cheung, W. Y., *Fed. Proc.* **1974**, *33*, 1391-1391.

150. Klee, C. B., *Biochemistry-Us* **1977**, *16*, 1017-1024.

151. Tsuruta, H.; Sano, T., *Biophys. Chem.* **1990**, *35*, 75-84.

152. Zhang, M.; Tanaka, T.; Ikura, M., *Nat. Struct. Mol. Biol.* **1995**, *2*, 758-767.

153. Qin, N.; Olcese, R.; Bransby, M.; Lin, T.; Birnbaumer, L., *Proc. Natl. Acad. Sci. U. S. A.* **1999**, *96*, 2435-2438.

154. Spring, K. R.; Davidson, M. W. Microscopyu: Http://www.microscopyu.com, vol. 2013.

155. Hess, D.; Isenberg, G., *FEBS Lett.* **1999**, *445*, 279-282.

156. Corrie, J. E.; Davis, C. T.; Eccleston, J. F., *Bioconj. Chem.* **2001**, *12*, 186-194.

157. Beatty, K. E.; Tirrell, D. A., *Bioorg. Med. Chem. Lett.* **2008**, *18*, 5995-5999.

158. Manning, H. C.; Smith, S. M.; Sexton, M.; Haviland, S.; Bai, M.; Cederquist, K.; Stella, N.; Bornhop, D. J., *Bioconjug. Chem.* **2006**, *17*, 735-740.

159. Ke, C. C.; Liu, R. S.; Suetsugu, A.; Kimura, H.; Ho, J. H.; Lee, O. K.; Hoffman, R. M., *Plos One* **2013**, *8*, e69658.

160. Ah Lee, S.; Ou, X.; Lee, J. E.; Yang, C., *Opt. Lett.* **2013**, *38*, 1817-1819.